© 2019. Published by The Company of Biologists Ltd | Development (2019) 146, dev174367. doi:10.1242/dev.174367

RESEARCH ARTICLE

Paxillin-dependent regulation of apical-basal polarity in mammary gland morphogenesis

Weiyi Xu[1], Anushree C. Gulvady[1,*], Gregory J. Goreczny[1,‡], Eric C. Olson[2] and Christopher E. Turner[1,§]

ABSTRACT

Establishing apical-basal epithelial cell polarity is fundamental for mammary gland duct morphogenesis during mammalian development. While the focal adhesion adapter protein paxillin is a well-characterized regulator of mesenchymal cell adhesion signaling, F-actin cytoskeleton remodeling and single cell migration, its role in epithelial tissue organization and mammary gland morphogenesis *in vivo* has not been investigated. Here, using a newly developed paxillin conditional knockout mouse model with targeted ablation in the mammary epithelium, in combination with *ex vivo* three-dimensional organoid and acini cultures, we identify new roles for paxillin in the establishment of apical-basal epithelial cell polarity and lumen formation, as well as mammary gland duct diameter and branching. Paxillin is shown to be required for the integrity and apical positioning of the Golgi network, Par complex and the Rab11/MyoVb trafficking machinery. Paxillin depletion also resulted in reduced levels of apical acetylated microtubules, and rescue experiments with the HDAC6 inhibitor tubacin highlight the central role for paxillin-dependent regulation of HDAC6 activity and associated microtubule acetylation in controlling epithelial cell apical-basal polarity and tissue branching morphogenesis.

KEY WORDS: Focal adhesions, Cell polarity, Tubulin acetylation, Vesicle trafficking, Cytoskeleton, Extracellular matrix

INTRODUCTION

Mammary gland morphogenesis is a complex process involving basement membrane remodeling, polarized lumen formation, ductal elongation and branching that is essential for establishing the appropriate tissue architecture necessary for subsequent milk production in the lactating adult (Andrew and Ewald, 2010; Muschler and Streuli, 2010). Mechanical signaling, integrin receptor-mediated cytoskeletal remodeling and polarized trafficking of intracellular organelles are tightly regulated to ensure proper development of the gland (Gjorevski and Nelson, 2010; Roignot et al., 2013; Schedin and Keely, 2011), although our understanding of how these events are integrated remains incomplete. During ductal elongation, branching can be achieved through a combination of cell proliferation and cell rearrangement, involving bifurcation, where the ends of the duct split into two ducts and/or side branching of the main duct (Andrew and Ewald, 2010; Lu et al., 2008). Cell-extracellular matrix (ECM) adhesion signaling plays several key roles during these branching events, including further regulation of fibronectin turnover (Kadoya and Yamashina, 2010; Simian et al., 2001) as well as remodeling of the actin cytoskeleton to influence epithelial cell morphology, cell-cell interactions and cell motility (Spurlin and Nelson, 2017). F-actin-associated actomyosin contractility is also crucial for mammary gland branching morphogenesis. For example, three-dimensional (3D) *in vitro* organoid culture studies showed that elevated Ras activity and enrichment of F-actin at the apical surface of the cell generated by mechanical gradients in the duct contributes to ductal elongation (Neumann et al., 2018), whereas inhibition of Rac-1 or myosin light chain kinase blocks organoid branching (Ewald et al., 2008).

Importantly, ECM-integrin signaling also regulates microtubule (MT) polymerization, in part by transducing signals from β1 integrin through integrin-linked kinase (ILK) to guide epithelial cell apical-basal polarity and duct lumen formation (Akhtar and Streuli, 2013). Lumen formation requires the establishment of columnar shaped cells with apical-basal polarity (Datta et al., 2011; Rodriguez-Fraticelli et al., 2011). This apical-basal cell polarity is accomplished through the polarized distribution of key plasma membrane components and cellular organelles including the Golgi complex (Rodriguez-Boulan and Macara, 2014). Polarized trafficking of the Par3-Par6-aPKC complex to the apical side of the epithelial cells further facilitates development of apical polarity (Ahmed and Macara, 2017; Bilder and Perrimon, 2000; Tepass et al., 1990) and, in turn, tissue morphogenesis (McCaffrey and Macara, 2009). During apical membrane domain formation, the small GTPase Rab11a is activated at apical protein-containing vesicles and stimulates the binding of class V myosin motor B (MyoVb) (Roland et al., 2011; Welz et al., 2014). MyoVb is an actin-based motor protein that carries vesicles from the MTs and drives their movement along the cortical actin network for the targeted delivery of membrane proteins to the apical surface (Kapitein et al., 2013). However, the mechanism by which vesicle trafficking along the MT and F-actin networks influence polarized lumen formation and potentially branching morphogenesis still needs to be assessed.

A number of cell-ECM-associated focal adhesion proteins, including β1 integrin, FAK and ILK, have each been shown to play crucial roles in mammary gland branching morphogenesis, lumen development and milk production (Akhtar and Streuli, 2006, 2013; van Miltenburg et al., 2009). In cultured mesenchymal cells, the focal adhesion scaffold protein paxillin interacts directly with FAK and ILK, and also possibly β1 integrin (Brown and Turner, 2004; Nikolopoulos and Turner, 2001; Turner and Miller, 1994), and plays a key role in coordinating cell-ECM signaling (Turner et al., 1990) to regulate cytoskeleton reorganization, particularly via

[1]Department of Cell and Developmental Biology, State University of New York Upstate Medical University, 750 East Adams Street, Syracuse, NY 13210, USA. [2]Department of Neuroscience and Physiology, State University of New York Upstate Medical University, 505 Irving Ave, Syracuse, NY 13210, USA.
*Present address: Dana-Farber Cancer Institute, Harvard Medical School, 450 Brookline Ave, Boston, MA 02115, USA ‡Present address: Division of Hematology, Department of Medicine, Brigham and Women's Hospital, 75 Francis St, Boston, MA 02115, USA.

§Author for correspondence (turnerce@upstate.edu)

C.E.T., 0000-0002-7210-4007

Received 28 November 2018; Accepted 3 April 2019

Development (2019) 146, dev174367. doi:10.1242/dev.174367

coordination of Rho GTPase family activity (Brown and Turner, 2004; Deakin and Turner, 2008; Turner, 2000). More recently, paxillin has been shown to regulate MT acetylation in mesenchymal cells via interaction with, and inhibition of, the cytoplasmic tubulin deacetylase HDAC6 (Deakin and Turner, 2014). Furthermore, this signaling axis revealed a key role for paxillin in the regulation of front-rear cell polarity via control of Golgi cohesion and positioning, as well as polarized vesicle trafficking to the leading edge of motile cells (Deakin and Turner, 2014; Dubois et al., 2018).

Our understanding of the role played by paxillin in mammalian development, possibly via regulation of cell polarity has been limited due to the embryonic lethality caused by constitutive ablation of the paxillin gene in mice (Hagel et al., 2002). To begin to address this gap in knowledge, we have generated a conditional paxillin knockout mouse model and used MMTV-driven cre recombinase to selectively ablate paxillin in the developing mammary gland epithelium. By using this conditional paxillin knockout animal model, combined with *in vitro* 3D organoid and 3D acini culture assays of isolated cells, we show that paxillin is essential for mammary gland branching morphogenesis and polarized lumen formation via its regulation of the apical-basal epithelial cell polarity machinery, primarily through control of HDAC6 activity and associated MT acetylation.

RESULTS

Paxillin is required for normal mammary gland branching morphogenesis

Constitutive ablation of paxillin expression in mice results in embryonic lethality (Hagel et al., 2002). Accordingly, in order to study the role of paxillin in mammary gland development, we generated a conditional knockout mouse model to ablate paxillin in mammary luminal epithelial cells. Paxillin floxed (paxillin$^{fl/fl}$) mice were engineered in which exon 2-5 of the paxillin gene was flanked by loxP sites, and this was bred with the constitutive MMTV-Cre line D transgenic mouse line to specifically deplete the floxed allele from the mouse mammary epithelial cells (paxillin$^{fl/fl}$;cre) (Wagner et al., 2001). Previous studies have shown that the MMTV-Cre-mediated recombination in this line occurs 3 weeks postnatally and that cre expression is confined primarily to the luminal epithelial cell population (Elias et al., 2015).

To determine how loss of paxillin affects mammary gland morphogenesis, whole-mount staining was performed on the fourth inguinal mammary glands at postnatal week 6 (corresponding to early puberty) (Fig. 1A). Paxillin$^{fl/fl}$;cre mice lacking paxillin had significantly fewer branches within the gland when compared with the control paxillin$^{+/+}$;cre mice (Fig. 1B). However, despite a consistent reduction in branching, there was no significant difference seen in the extent of ductal penetration (Fig. 1C), stalk length between end buds or the number of terminal end buds (TEBs) (Fig. S1). Interestingly, measurement of the duct diameter in the whole-mount tissue at the same distance from the lymph node indicated that the paxillin$^{fl/fl}$;cre mice had larger ducts (Fig. 1Ai,Aii, D). Furthermore, histological analysis using Hematoxylin and Eosin staining (H&E) of glands of 6-week-old mice confirmed the dilated duct phenotype in the paxillin$^{fl/fl}$;cre mice (Fig. 1E,F). Immunostaining of cryosections from glands of 6-week-old mice revealed a primarily cytosolic distribution of paxillin in the paxillin$^{+/+}$;cre luminal epithelial cells and confirmed that paxillin was absent from the luminal epithelial cells of the paxillin$^{fl/fl}$;cre mice (Fig. 1G). In contrast to active integrin β1 (Fig. S2A) (Akhtar and Streuli, 2013), there was no obvious enrichment of paxillin at the basement membrane in the paxillin$^{+/+}$;cre ducts. However, both the distribution of active integrin β1, the level of pFAK and the level of laminin staining in the underlying ECM were perturbed in the ducts of the paxillin$^{fl/fl}$;cre mice (Fig. S2), suggesting a role for paxillin in cell-ECM signaling. PCR and western blotting analysis further confirmed appropriate cre-mediated recombination and paxillin protein depletion in the paxillin$^{fl/fl}$;cre mice (Fig. 1H). Taken together, these data indicate that paxillin deficiency alters duct size and branching morphogenesis during early mammary gland development.

Paxillin is required for mammary epithelial cell shape and cytoskeletal organization

To determine whether the observed phenotype within the mammary glands could have been caused by proliferation or apoptosis defects within the ducts, the mammary glands were stained for the proliferation marker Ki67 or the apoptotic marker cleaved caspase 3. However, no significant differences in the number of proliferating cells or cells undergoing apoptosis was observed (Fig. S3). The mammary stem cells are crucial for development, maintenance and regeneration of the epithelium, as they give rise to more stem cells or differentiated epithelial cells through symmetric and asymmetric divisions (Lloyd-Lewis et al., 2017). Thus, we also stained mammary gland sections for the stem cell marker-slug (Guo et al., 2012), but no obvious difference in either the number or location of slug-positive cells was observed (data not shown), suggesting that cell stemness is not affected by paxillin knockout.

Cell architecture and polarity have been shown to be crucial for branching and lumen formation (Spurlin and Nelson, 2017). Therefore, to determine whether there were any changes in epithelial tissue organization, the sections were stained for the tight junction marker ZO-1 as well as for the basolateral epithelial marker EpCAM. Measurement of the aspect ratio (apical cell width versus cell height) of the epithelial cells lining the lumen, indicated that unlike control animals that have a predominantly columnar-like cell shape, the paxillin$^{fl/fl}$;cre luminal epithelial cells were either cuboidal or exhibited a more elongated, flattened cell morphology (Fig. 2A,B).

The F-actin and microtubule-based cytoskeleton networks play crucial roles in determining cell shape, and therefore in facilitating branching morphogenesis (Akhtar and Streuli, 2013; Spurlin and Nelson, 2017). Staining the sections with phalloidin revealed that the F-actin organization was substantially disrupted in the paxillin$^{fl/fl}$;cre glands (Fig. 2C,D). In the control paxillin$^{+/+}$;cre glands the F-actin localized uniformly to the apical surface (Fig. 2C, asterisk) and was also enriched in the underlying myoepithelial layer (arrow), whereas in cells in the paxillin$^{fl/fl}$;cre glands, apical F-actin-rich membrane blebs formed, suggesting either paxillin-dependent defects in F-actin organization and/or stabilization of the apical membrane domain (Fig. 2C,D). To assess whether the F-actin disorganization may also be associated with differences in acto-myosin-based contractile forces, western blotting analysis was performed on isolated mammary epithelial tissue using the contractility marker phospho-myosin light chain (pMLC). The pMLC levels in paxillin$^{fl/fl}$;cre mammary glands was significantly reduced, suggesting that paxillin$^{fl/fl}$;cre mammary epithelial cells may be less contractile (Fig. 2E).

The microtubule (MT) network has been previously shown to be crucial for mammary gland morphogenesis through its role in the establishment of epithelial cell polarity (Akhtar and Streuli, 2013). To examine whether the MT network is disrupted in the paxillin-depleted mammary glands, tissue sections were stained for α-tubulin. However, the α-tubulin staining showed no obvious differences in global MT distribution or mean fluorescence intensity

Development (2019) 146, dev174367. doi:10.1242/dev.174367

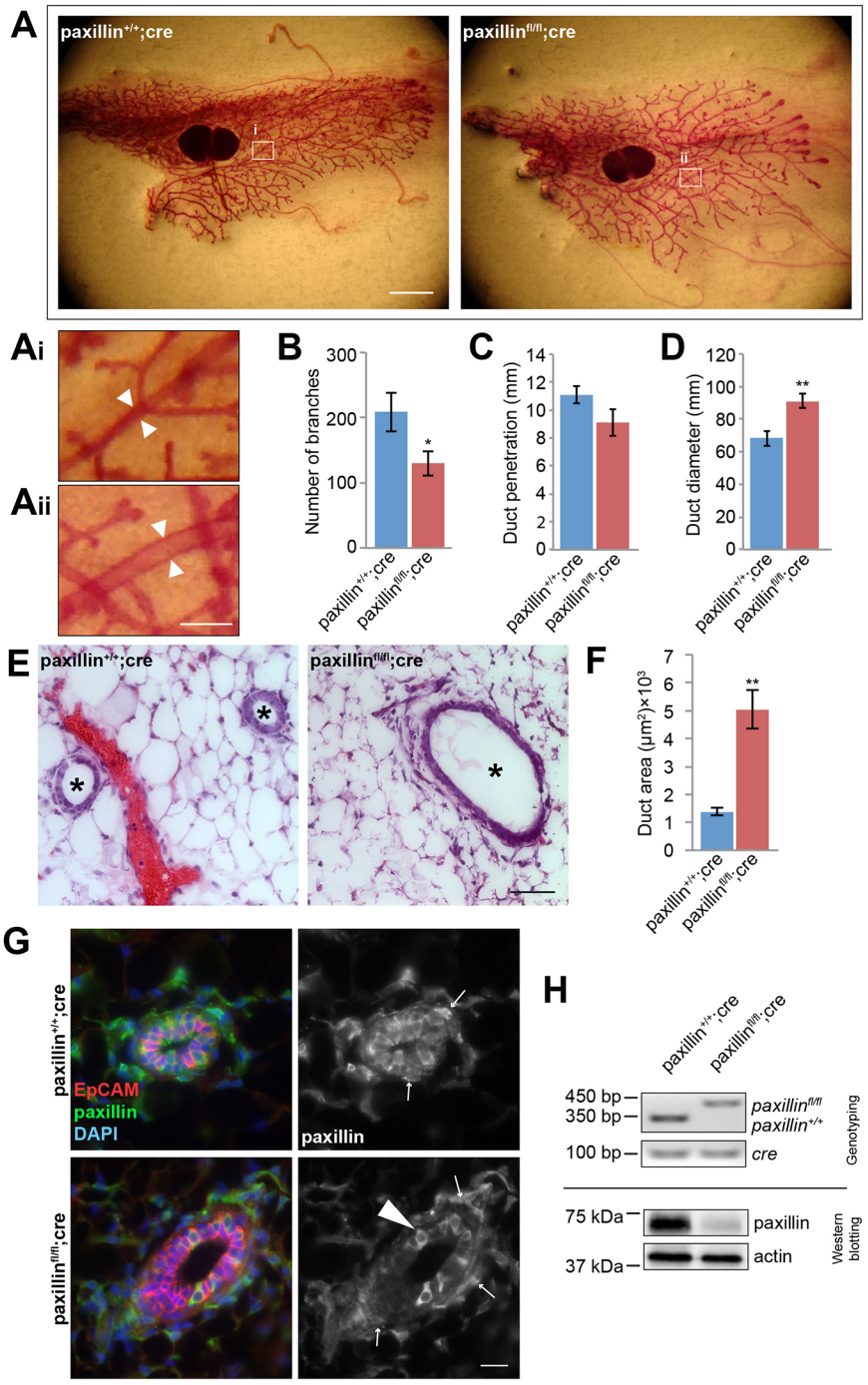

Fig. 1. Paxillin$^{fl/fl}$cre mammary glands have fewer branches and dilated ducts. (A) Whole-mount staining of 6-week-old paxillin$^{+/+}$;cre and paxillin$^{fl/fl}$;cre mammary glands. Scale bar: 2 mm. (Ai,Aii) Higher-magnification images showing that paxillin$^{fl/fl}$;cre have larger duct diameters (arrowheads). Scale bar: 250 µm. (B) Quantification of the total number of branches in the mammary gland, *n*=10 animals (paxillin$^{+/+}$;cre), *n*=13 (paxillin$^{fl/fl}$;cre). (C) Quantification of duct penetration. *n*=6 (paxillin$^{+/+}$;cre), *n*=8 (paxillin$^{fl/fl}$;cre). (D) Quantification of duct diameter, *n*=6 (paxillin$^{+/+}$;cre), *n*=7 (paxillin$^{fl/fl}$;cre). (E) Hematoxylin and Eosin staining of 6-week-old mammary gland sections. Asterisks indicate individual ducts. Scale bar: 50 µm. (F) Quantification of duct cross-section area, *n*=3 (paxillin$^{+/+}$;cre), *n*=5 (paxillin$^{fl/fl}$;cre). (G) Paxillin expression pattern in 6-week-old mammary glands. Occasional mosaic expression of paxillin was observed in paxillin$^{fl/fl}$;cre glands (arrowhead). Arrows indicate myoepithelial cells. Scale bar: 20 µm. (H) Genotyping from mice tail snips and western blotting of paxillin using lysates obtained from mammary gland extract. Student's *t*-test was performed. Data are mean±s.e.m. $^{**}P<0.01$.

(MFI) between paxillin$^{+/+}$;cre and paxillin$^{fl/fl}$;cre mammary glands (Fig. S4). Importantly, MTs undergo various post-translational modifications that affect their function (Song and Brady, 2015) and MT acetylation has been shown to be associated with apical constriction (contractility) of epithelial cell layers in *Drosophila* and polarized trafficking in 2D cell culture systems (Booth et al., 2014; Deakin and Turner, 2014; Fernandes et al., 2014). However, to our knowledge, the role of MT acetylation has not previously been evaluated in mammary gland morphogenesis. Interestingly, immunostaining for acetylated tubulin revealed that MT acetylation was perturbed in the paxillin$^{fl/fl}$;cre mammary glands (Fig. 2F). In the paxillin$^{+/+}$;cre glands, the MTs were highly acetylated and enriched at the apical side of the duct, whereas the staining in the luminal epithelial cells of the paxillin$^{fl/fl}$;cre mammary glands was more diffuse throughout the cells (Fig. 2F,G). Western blotting analysis for acetylated tubulin using lysates obtained from both paxillin$^{+/+}$;cre and paxillin$^{fl/fl}$;cre mammary glands showed reduced levels of acetylated-tubulin in the paxillin$^{fl/fl}$;cre mammary glands when compared with the paxillin$^{+/+}$;cre glands (Fig. 2H), indicating that paxillin is required for MT acetylation and possibly its spatiotemporal regulation during mammary gland morphogenesis. Taken together, these data highlight crucial roles for paxillin in coordinating both F-actin cytoskeleton organization and MT acetylation, which likely contributes to the acquisition and maintenance of normal mammary epithelial cell shape.

Development (2019) 146, dev174367. doi:10.1242/dev.174367

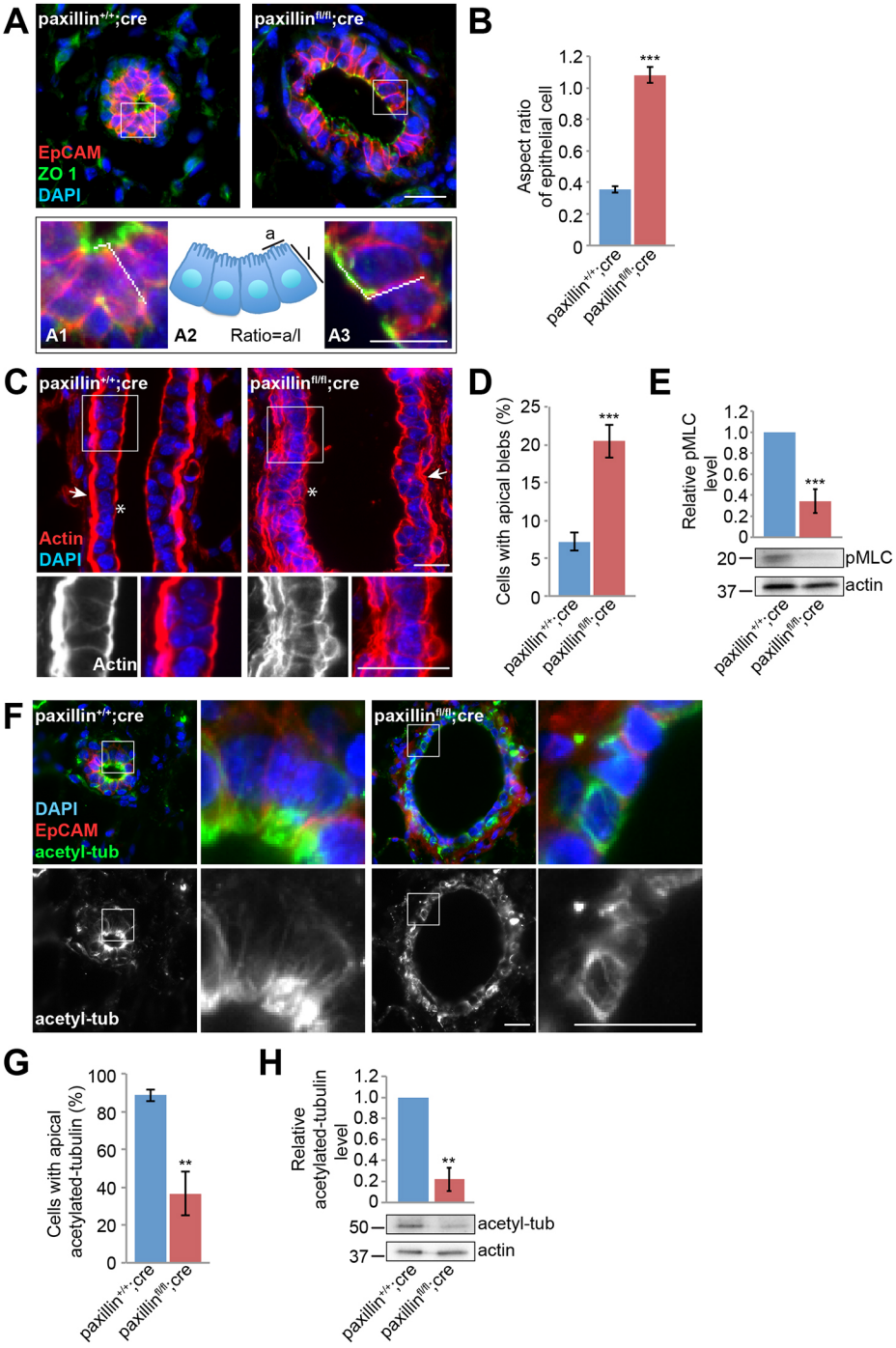

Fig. 2. Paxillin$^{fl/fl}$cre mammary glands have disrupted epithelial cell shape and disorganized cytoskeletal components. (A) Six-week-old mammary gland sections labeled for the tight junction marker ZO1 and the baso-lateral membrane marker EpCAM. Higher magnification of the boxed areas are shown in (A1) paxillin$^{+/+}$;cre and (A3) paxillin$^{fl/fl}$;cre. (A2) Schematic of the apical and lateral cell membrane measurements used for calculating ratios. Scale bars: 20 µm. (B) Quantification of apical-to-lateral membrane length ratio, n=3 (at least 20 cells per animal). (C) Actin staining of longitudinal sections of mammary gland ducts. Asterisks indicate the apical surface; arrows indicate the myoepithelial layer. Scale bars: 20 µm. (D) Quantification of the number of cells with apical F-actin blebs, n=6 (paxillin$^{+/+}$;cre), n=7 (paxillin$^{fl/fl}$;cre) (at least three ducts per animal). (E) Mammary epithelial cell lysates blotted for pMLC and quantification of the relative level, normalized to actin. (F) Six-week-old mammary gland stained for acetylated tubulin. Scale bars: 20 µm. (G) Quantification of cells with apical acetylated tubulin, n=5 (paxillin$^{+/+}$;cre), n=4 (paxillin$^{fl/fl}$;cre) (at least 28 cells per animal). (H) Mammary epithelial cell lysates blotted for acetylated tubulin and quantification of the relative expression level. Student's t-test was performed. Data are mean±s.e.m. $^{**}P$<0.01, $^{***}P$<0.001.

Paxillin is indispensable for the positioning of apical proteins and ductal apical-basal polarity in the developing mammary gland

Subapical localization of the Golgi apparatus facilitates apical vesicle trafficking and thus promotes polarization of the mammary epithelium (Datta et al., 2011; Roignot et al., 2013). Previously, we have shown that paxillin, through regulation of MT acetylation, is required for maintaining the positioning and integrity of the Golgi apparatus, as well as regulation of front-rear polarized trafficking in MDA-MB-231 breast cancer cells and normal fibroblasts (Deakin and Turner, 2014; Dubois et al., 2018). As the luminal epithelial cells of paxillin$^{fl/fl}$;cre mammary glands have dysregulated cell shape (Fig. 2A,B) and disrupted MT acetylation (Fig. 2F-H), we assessed whether apical-basal polarity is also affected in the absence of paxillin. Mammary gland sections were stained with the *trans*-Golgi marker giantin and line profile analyses were performed to quantify the distribution of the Golgi apparatus. Compared with the apical distribution of the Golgi apparatus in paxillin$^{+/+}$;cre mammary glands, the Golgi apparatus in paxillin$^{fl/fl}$;cre mammary glands exhibited a dispersed distribution throughout the cytoplasm (Fig. 3A-C). Polarized lumen formation requires apical positioning of the Par and Crumbs protein complexes (Kim et al., 2018). Staining for Par3 revealed the typical apical localization in the paxillin$^{+/+}$;cre mammary glands, while the paxillin$^{fl/fl}$;cre mammary glands exhibited both apical and basal-lateral Par3 staining (Fig. 3D,E), further

Development (2019) 146, dev174367. doi:10.1242/dev.174367

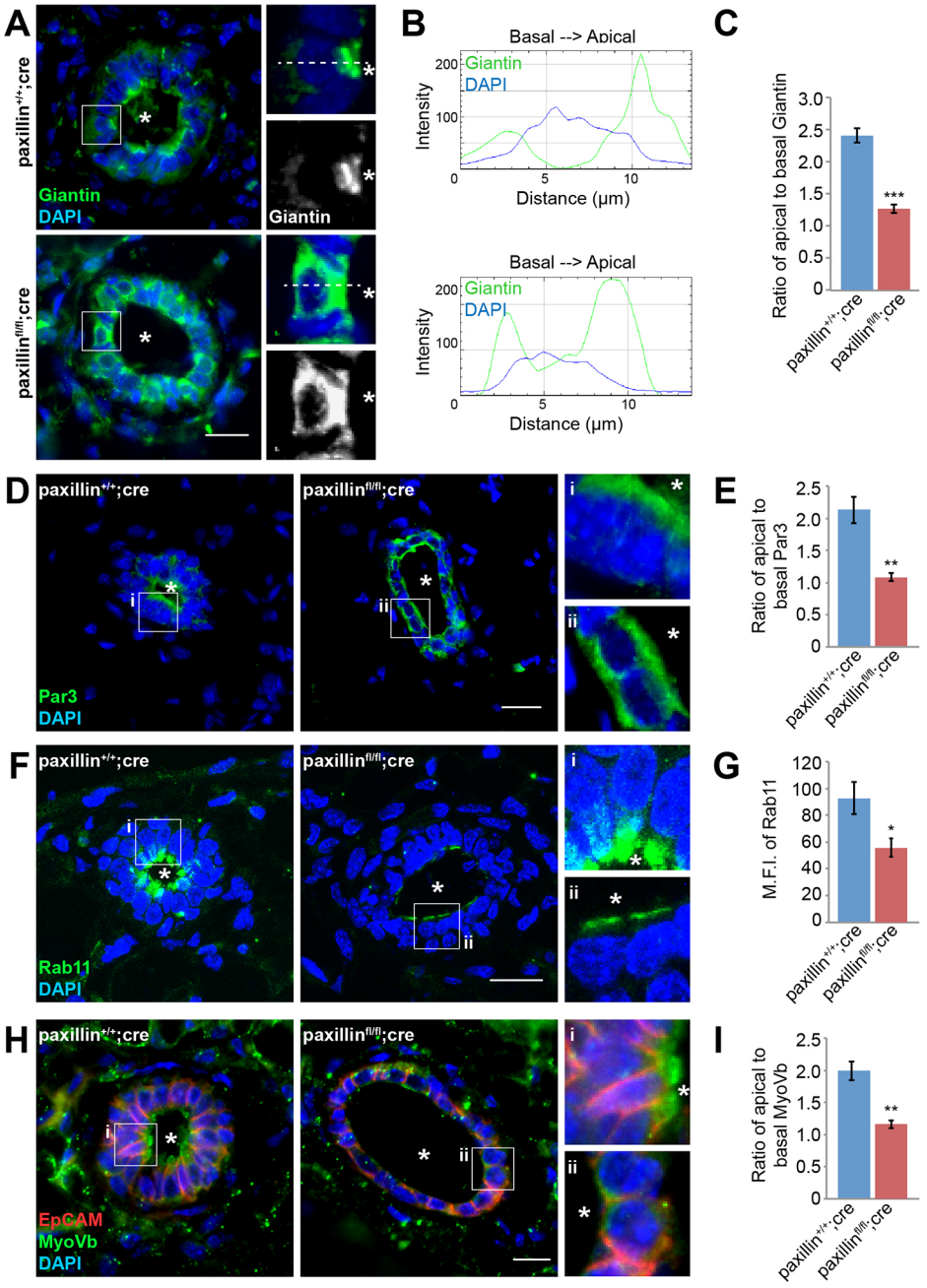

Fig. 3. Cell polarity and the apical trafficking complex are disrupted in paxillin$^{fl/fl}$cre mammary glands. (A) Mammary gland sections stained for the Golgi marker giantin. Scale bar: 20 µm. (B) Line profiles showing Golgi distribution, using ImageJ. (C) Quantification of Golgi distribution: the ratio of maximal fluorescence intensity at the apical side versus the maximal fluorescence intensity at the basal side, *n*=3 (at least 4 ducts per animal, at least 10 cells per duct). (D) Tissue sections stained for the apical marker Par3. Scale bar: 20 µm. (E) Quantification of Par3 distribution: the ratio of maximal fluorescence intensity at the apical side versus the maximal fluorescence intensity at the basal side, *n*=3 (at least 3 ducts per animal, at least seven cells per duct). (F) Tissue sections stained for the apical recycling-associated trafficking marker Rab11. Scale bar: 20 µm. (G) Quantification of mean fluorescence intensity of Rab11, *n*=3 (at least three ducts per animal). (H) Tissue sections stained for the apical trafficking motor protein MyoVb. Scale bar: 20 µm. Asterisks in the images indicate individual ducts. (I) Quantification of MyoVb distribution. Student's *t*-test was performed. Data are mean ±s.e.m. **P*<0.05, ***P*<0.01, ****P*<0.001.

indicating that paxillin expression is necessary for establishing apical-basal polarity in the luminal epithelial cells.

To determine whether the disrupted apical-basal polarization seen in the paxillin$^{fl/fl}$;cre glands is associated with defective apical protein trafficking, mammary gland sections were immunostained for the apical trafficking-associated Rab GTPase protein, Rab11 and its associated motor protein MyoVb (Roland et al., 2011). Interestingly, the distribution of both Rab11 and MyoVb was perturbed in the paxillin$^{fl/fl}$;cre glands. In comparison with paxillin$^{+/+}$;cre glands, where robust apical staining was observed, although still apically localized, the paxillin$^{fl/fl}$;cre glands had substantially reduced levels of Rab11 (Fig. 3F,G; Fig. S5A,C). MyoVb distribution was examined by immunostaining and line profile analysis, and instead of the apical MyoVb distribution seen in paxillin$^{+/+}$;cre glands, the MyoVb in the paxillin$^{fl/fl}$;cre glands had a less polarized, dispersed distribution (Fig. 3H,I). However, western blot analysis showed the expression level of MyoVb was unchanged in paxillin$^{fl/fl}$;cre glands (Fig. S5A,B). Taken together, these data indicate a key role for paxillin is establishing apical-basal polarity in mammary gland epithelia to promote apical protein trafficking.

Paxillin is required for polarized acini formation in 3D culture

The *in vivo* mouse studies demonstrate that luminal epithelia of the paxillin$^{fl/fl}$;cre mammary glands fail to polarize (Fig. 3). To begin to explore the underlying mechanism(s), we used the 3D acini culture system, which serves as a useful model for studying epithelial cell polarity *in vitro* (Bryant et al., 2014). Isolated luminal epithelial cells are able to form acini with a single apical-basal polarized cell layer surrounding a central lumen when plated on Matrigel-coated substrates (Fig. 4A) (Akhtar et al., 2009). To assess whether paxillin expression regulates that ability of mammary epithelial cells (MECs) to form polarized acini, 6-day 3D-cultured MECs

Development (2019) 146, dev174367. doi:10.1242/dev.174367

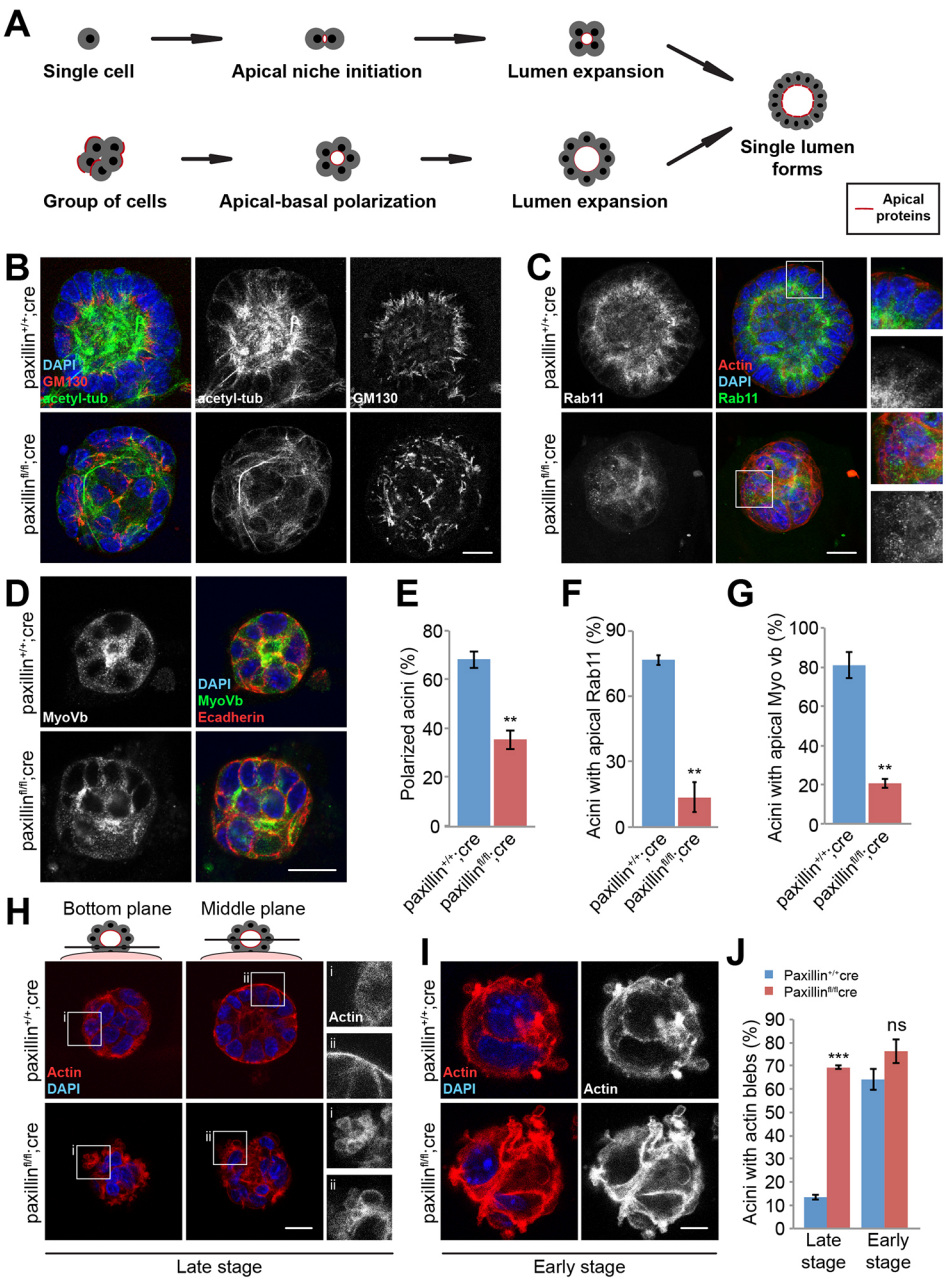

Fig. 4. Paxillin$^{fl/fl}$cre mammary epithelial cells are not able to form polarized acini in 3D matrigel culture. (A) Schematic of cells forming polarized acini. (B) Six-day-old acini stained for acetylated-tubulin and the Golgi marker GM130. Scale bar: 5 µm. (C) Six-day-old acini stained for Rab11. Scale bar: 5 µm. (D) Six-day-old acini stained for MyoVb and E-cadherin. Scale bar: 5 µm. (E) Quantification of cells forming polarized acini (more than 90% of the cells with apical Golgi), *n*=3 (total of 36-165 acini per genotype). (F) Quantification of acini with apical Rab11 distribution, *n*=3. (G) Quantification of acini with apical MyoVb distribution, *n*=3. (H) Six-day-old acini stained for F-actin. Scale bar: 5 µm. (I) Two-day-old acini stained for F-actin. Scale bar: 2 µm. (J) Quantification of acini with basal F-actin-containing blebs, *n*=3 (total of 26-74 acini per genotype). Student's *t*-test was performed. Data are mean±s.e.m. ns, not significant; $^{**}P<0.01$, $^{***}P<0.001$.

isolated from control and knockout mice were stained with the apical marker GM130. In contrast to paxillin$^{+/+}$;cre MECs, which formed polarized acini with a central lumen and apical GM130 distribution, paxillin$^{fl/fl}$;cre MECs formed disorganized cell spheres lacking a central lumen and a clearly defined apical surface (Fig. 4B,E). Staining with the tight junction marker ZO1 also confirmed the significant lack of a central lumen in the paxillin$^{fl/fl}$;cre acini ($P<0.01$). Interestingly, the paxillin$^{fl/fl}$;cre cells also produced more multi-lumen acini than the paxillin$^{+/+}$;cre MECs, but this difference was not significant ($P=0.34$) (Fig. S6).

Previous studies have shown that integrin-dependent MT network alignment is crucial for directed trafficking of apical proteins and the formation of polarized acini (Akhtar and Streuli, 2013). However, the role of MT acetylation in regulating apical domain formation has not been evaluated. Given that the paxillin$^{fl/fl}$;cre mammary glands have reduced enrichment of apically distributed acetylated tubulin (Fig. 2F-H), we assessed whether paxillin$^{fl/fl}$;cre MECs also demonstrated a reduced apical MT acetylation in the 3D acini culture. Consistent with the *in vivo* results, paxillin$^{+/+}$;cre acini exhibited apically positioned acetylated MTs, whereas acetylated MT staining was more disorganized and reduced by 40.3% ($P<0.05$) in the paxillin$^{fl/fl}$;cre acini (Fig. 4B; Movies 1 and 2). Immunostaining the acini for paxillin confirmed its absence from the paxillin$^{fl/fl}$;cre acini (Fig. S7A).

To assess whether the 3D acini culture recapitulated the *in vivo* phenotype in which apical trafficking was disrupted in paxillin$^{fl/fl}$;cre mammary glands, the acini were immunostained for Rab11 and MyoVb. Compared with the apically localized Rab11 and MyoVb in paxillin$^{+/+}$;cre acini, the paxillin$^{fl/fl}$;cre acini exhibited non-polarized distribution of both Rab11 or MyoVb (Fig. 4C,D,F,G). The MFI of Rab11 was also reduced by 39.6±4.14% (±s.e.m.) in the paxillin$^{fl/fl}$;cre acini. The FM4-64 dye was also used to analyze baso-lateral to apical membrane trafficking (Elias et al., 2015). Time-lapse imaging showed that the FM4-64 dye accumulated at

Development (2019) 146, dev174367. doi:10.1242/dev.174367

the apical membrane in paxillin$^{+/+}$;cre acini, but the paxillin$^{fl/fl}$;cre acini failed to demonstrate a similar apical accumulation (Fig. S7B). Together, these data establish a key role for paxillin in organizing the MT cytoskeleton and apical membrane trafficking machinery required for polarized acini formation.

F-actin blebs and a reduced level of pMLC were observed in the paxillin$^{fl/fl}$;cre glands (Fig. 2C-E), suggesting a role for paxillin in regulating epithelial cell F-actin organization and cell contractility. Similarly, phalloidin staining of the paxillin$^{fl/fl}$;cre acini revealed significantly more F-actin-rich membrane blebs when compared with control paxillin$^{+/+}$;cre acini, confirming that paxillin is also required for F-actin organization and function in 3D acini culture (Fig. 4H,J; Movies 3 and 4). Interestingly, when early stage acini (fewer than eight cells) were stained for phalloidin, a similar number of both paxillin$^{+/+}$;cre and paxillin$^{fl/fl}$;cre acini formed basal F-actin blebs, which preceded central lumen formation in the paxillin$^{+/+}$;cre acini (Fig. 4I,J; Movies 5 and 6), suggesting that these early F-actin blebs may be a part of normal mammary acinus formation and that paxillin is crucial for suppressing the F-actin blebs in fully polarized acini.

Paxillin facilitates polarized lumen formation by inhibiting HDAC6 activity

We have previously reported that, in cultured fibroblasts and MDA-MB-231 breast tumor cells, paxillin binds to and inhibits HDAC6 activity to regulate MT acetylation to control mesenchymal cell front-rear polarity (Deakin and Turner, 2014). We therefore hypothesized that paxillin-dependent differences in MT acetylation observed in both the mammary gland *in vivo* (Fig. 2F) and in the acini *in vitro* (Fig. 4B) may also be regulated through paxillin-HDAC6 inhibition and would be crucial for polarized lumen formation. Western blotting analysis was performed for HDAC6 expression using epithelial cell lysates isolated from both paxillin$^{+/+}$;cre and paxillin$^{fl/fl}$;cre mammary glands, and consistent with the outcome in mesenchymal cells, HDAC6 expression was unchanged (Fig. 5A). To modulate HDAC6 activity, paxillin$^{+/+}$;cre and paxillin$^{fl/fl}$;cre acini were treated with the HDAC6-specific inhibitor tubacin (Haggarty et al., 2003) and evaluated for cell polarization and lumen formation. Strikingly, the tubacin-treated paxillin$^{fl/fl}$;cre acini formed similar numbers of acini with polarized GM130 Golgi staining and a central lumen as DMSO or tubacin-treated paxillin$^{+/+}$;cre acini (Fig. 5B,C). These data demonstrate that suppression of HDAC6 activity is sufficient to rescue polarized lumen formation in the absence of paxillin. Interestingly, HDAC6 inhibition also rescued the polarization defect of the apical trafficking machinery in paxillin$^{fl/fl}$;cre acini, as indicated by the restoration of an apical distribution of both Rab11 and MyoVb staining following tubacin treatment (Fig. 5D-G).

Line profile analysis of the acetylated tubulin staining revealed that, following tubacin treatment, the fluorescence intensity towards the apical surface of the paxillin$^{fl/fl}$;cre acini was comparable with the acetylated MT levels observed in DMSO or drug-treated paxillin$^{+/+}$;cre acini, whereas the levels of acetylated MTs at the basal side were similarly elevated in both cell populations (Fig. S8).

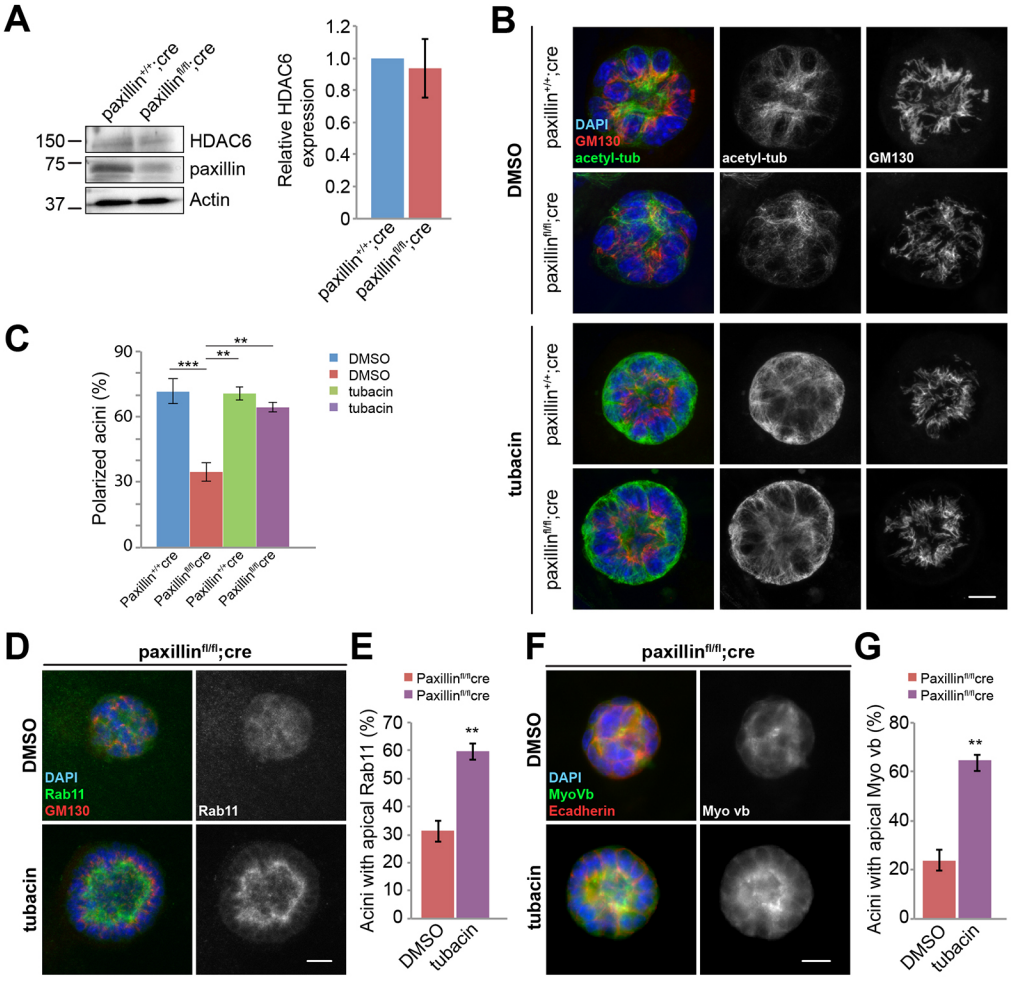

Fig. 5. HDAC6 inhibition rescues the ability of paxillin$^{fl/fl}$cre cells to form polarized acini. (A) Mammary epithelial cell lysates blotted for HDAC6 and paxillin. Quantification of HDAC6 from five different blots from three sets of animals. (B) Paxillin$^{+/+}$;cre and paxillin$^{fl/fl}$;cre acini were treated with 2 µM tubacin, followed by staining for acetylated tubulin and GM130. Scale bar: 5 µm. (C) Quantification of polarized acini, *n*=3 (total of 15-93 acini per treatment). One-way ANOVA with Tukey's multiple comparisons test was performed for statistical analysis. (D) Tubacin-treated paxillin$^{fl/fl}$;cre acini stained for Rab11 and GM130. Scale bar: 5 µm. (E) Quantification of acini with apical Rab11, *n*=3 (total of 11-144 acini per treatment). (F) Tubacin-treated paxillin$^{fl/fl}$;cre acini stained for MyoVb and E-cadherin. Scale bar: 5 µm. (G) Quantification of acini with apical MyoVb, *n*=3 (total of 14-89 acini per treatment). Student's *t*-test was performed. Data are mean±s.e.m. $^{**}P<0.01$, $^{***}P<0.001$.

Development (2019) 146, dev174367. doi:10.1242/dev.174367

Together, these data suggest that an elevated level of MT acetylation towards the apical surface is most important for establishing acini polarization.

Paxillin is required for *ex vivo* 3D organoid branching morphogenesis

Paxillin depletion in the mammary epithelium resulted in a decrease in ductal branching *in vivo* (Fig. 1A,B). To further examine the mechanism by which paxillin regulates branching morphogenesis, we used an *ex vivo* 3D organoid culture model system (Fig. 6A) (Ewald et al., 2008). Time-lapse imaging of Matrigel-embedded organoids for 7 days revealed that, although the paxillin$^{fl/fl}$;cre organoids were able to survive and proliferate, they failed to branch as efficiently as paxillin$^{+/+}$;cre organoids (Fig. 6B,C; Movies 7 and 8). Examination of the whole-mount organoids stained for paxillin confirmed its expression in the paxillin$^{+/+}$;cre organoids

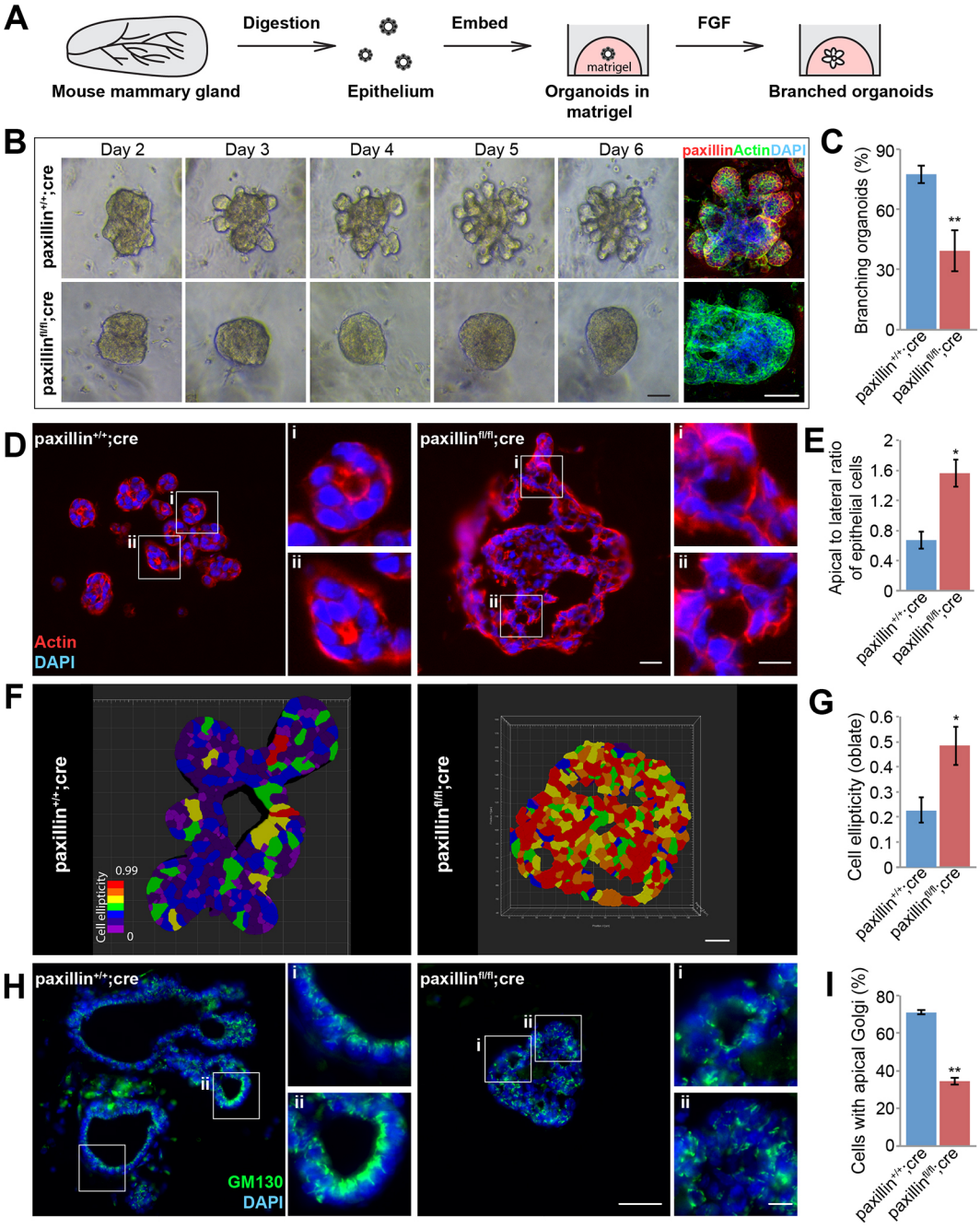

Fig. 6. Paxillin$^{fl/fl}$cre mouse-derived organoids are unable to branch efficiently, have disrupted cell polarity and altered cell ellipticity. (A) Schematic of organoid branching morphogenesis assay. (B) Time-lapse phase imaging montage of paxillin$^{+/+}$;cre and paxillin$^{fl/fl}$;cre organoids growing in 3D matrigel for 6 days. Whole mount of day 6 organoids stained for paxillin. Scale bars: 40 µm. (C) Quantification of organoid branching, n=5. (D) Day 6 organoid sections stained for F-actin to visualize apical-lateral length ratio. Scale bars: 20 µm; 4 µm in higher magnifications. (E) Quantification of apical-to-lateral ratio, n=3 (at least 10 cells per organoid). (F) Imaris analysis showing a single optical section through the day 6 organoids. Scale bar: 20 µm. (G) Quantification of 3D cell ellipticity (oblate), n=3 (at least 200 cells per organoid). (H) Day 6 organoid sections stained for the Golgi marker GM130. Scale bars: 50 µm; 10 µm in higher magnifications. (I) Quantification of cells with apical GM130 Golgi staining, n=3 (at least 20 cells per organoid). Student's t-test was performed. Data are mean±s.e.m. *P<0.05, **P<0.01.

Development (2019) 146, dev174367. doi:10.1242/dev.174367

and that the unbranched paxillin$^{fl/fl}$;cre organoids lacked paxillin (Fig. 6B).

To determine whether paxillin$^{fl/fl}$;cre organoids recapitulated other defects observed *in vivo*, organoid sections were immunostained for F-actin to examine cell shape. Quantification of the cell aspect ratio showed that the paxillin$^{+/+}$;cre organoids contained primarily columnar shaped cells, whereas the paxillin$^{fl/fl}$;cre cells were more flattened (Fig. 6D,E). In addition, 3D cell shape analysis using an Imaris cell membrane detection algorithm revealed that paxillin$^{fl/fl}$;cre cells had a higher cell oblate ellipticity, indicative of a disk-like spheroid (Fig. 6F,G). This result is consistent with the *in vivo* observation that paxillin$^{fl/fl}$;cre cells are more flattened when compared with paxillin$^{+/+}$;cre cells (Fig. 2A,B). To evaluate whether cell polarity was also disrupted in the paxillin$^{fl/fl}$;cre organoids, organoid sections were stained for the *cis*-Golgi marker GM130. Consistent with the phenotype observed *in vivo*, the GM130 was localized apically in the paxillin$^{+/+}$;cre organoids but was more dispersed in the paxillin$^{fl/fl}$;cre organoids (Fig. 6H,I), While the paxillin$^{+/+}$;cre organoids also formed a single lumen in association with their branched and polarized epithelial cell layers, the paxillin$^{fl/fl}$;cre organoids generally formed solid balls of cells lacking a central lumen or formed multiple small lumens similar to the acini. Taken together, these data suggest that paxillin-dependent cell shape and the acquisition/maintenance of cell polarity is necessary for organoid branching morphogenesis.

As lower pMLC levels were observed in the paxillin$^{fl/fl}$;cre mammary gland tissue (Fig. 2E), suggesting paxillin-dependent defects in contractility, we sought to examine whether paxillin-mediated contractile forces are important for mammary organoid branching. Paxillin$^{+/+}$;cre and paxillin$^{fl/fl}$;cre organoids were therefore treated with the myosin II inhibitor blebbistatin. However, instead of causing a reduction in branching that mimicked the untreated paxillin$^{fl/fl}$;cre organoids, the blebbistatin-treated paxillin$^{+/+}$;cre organoids actually formed a hyperbranched phenotype with an increase in peripheral cell protrusiveness (Fig. S9A). Similar hyperbranching results have been obtained using the Rho kinase (ROCK) inhibitor (Y-27632) (Ewald et al., 2008 and data not shown). Although the blebbistatin-treated paxillin$^{fl/fl}$;cre organoids also exhibited increased membrane protrusion activity, they remained unable to branch (Fig. S9A,B). These data indicate that the contractility defect seen in the paxillin$^{fl/fl}$;cre mammary gland, although likely involved in controlling cell shape, may not be directly associated with the branching deficiency.

Inhibition of HDAC6 rescues the organoid-branching defect caused by paxillin depletion

Epithelial cell rearrangement, polarity and cell organization is crucial for branching morphogenesis (Andrew and Ewald, 2010). Therefore, based on the ability of HDAC6 inhibition to rescue acini polarity and lumen formation in the absence of paxillin, we hypothesized that paxillin-HDAC6-dependent regulation of MT acetylation is also a prerequisite for branching morphogenesis. Accordingly, organoids were treated with tubacin. Although the DMSO-treated paxillin$^{fl/fl}$;cre organoids lacking paxillin failed to branch, tubacin treatment resulted in a significant rescue of branching morphogenesis in these organoids to levels comparable with control paxillin$^{+/+}$;cre organoids (Fig. 7A,B; Movies 9 and 10). Organoids stained for acetylated tubulin to assess tubacin-mediated HDAC6 inhibition showed that the MTs were highly acetylated after tubacin treatment in both paxillin$^{+/+}$;cre and paxillin$^{fl/fl}$;cre organoids (Fig. 7C). Immunostaining for paxillin was performed to confirm the absence of paxillin expression in tubacin-treated paxillin$^{fl/fl}$;cre organoids (Fig. S9C). To evaluate the specific role of MT acetylation versus other mechanisms that may impact MT stability, paxillin$^{fl/fl}$;cre organoids were similarly treated with the MT-stabilizing drug paclitaxel (Akhtar and Streuli, 2013). Interestingly, paclitaxel was not able to rescue branching in these paxillin-deficient organoids and also blocked branching in the paxillin$^{+/+}$;cre organoids (Fig. 7D,E; Fig. S10A,B), indicating that MT stabilization per se is not sufficient to rescue the branching defect. Conversely, to evaluate whether the branching defect seen in paxillin$^{fl/fl}$;cre organoids may be caused by MT destabilization, organoids were treated with the MT-disrupting drug nocodazole (Akhtar and Streuli, 2013). Predictably, nocodazole treatment did not induce branching in the paxillin$^{fl/fl}$;cre organoids. However, the nocodazole-treated paxillin$^{+/+}$;cre organoids, while failing to undergo branching, displayed a dose-dependent rounded morphology with loosely attached cells (Fig. 7D; Fig. S10C), suggesting that the nocodazole-induced defect is different from the phenotype seen with paxillin depletion alone. Taken together, these data indicate that paxillin-HDAC6-regulated MT acetylation, but not MT stabilization or destabilization alone, is key for organoid branching morphogenesis.

DISCUSSION

Herein, we have evaluated the role of paxillin in mouse mammary gland morphogenesis by using a recently generated conditional knockout mouse model and selectively ablating paxillin in the luminal epithelial cells of the mouse mammary gland. Of importance, this model provides the first evidence for paxillin-dependent regulation of epithelial cell and tissue organization *in vivo*, including control of cell polarity and shape, lumen formation and ductal branching. Although paxillin-dependent perturbations in the F-actin cytoarchitecture were also observed, using *ex vivo* 3D organoid and *in vitro* acini primary culture model systems to further dissect the underlying mechanism(s), we have identified a primary role for paxillin-mediated regulation of HDAC6 activity and associated microtubule (MT) acetylation in defining these tissue characteristics (Fig. 8). Thus, the paxillin-HDAC6-MT acetylation signaling axis appears to define a common mechanism for coordinating the organization of the cell polarity machinery in both epithelial (apical-basal) (this study) and mesenchymal (front-rear) (Deakin and Turner, 2014) cell types.

The major morphological defects observed in the paxillin$^{fl/fl}$;cre mammary glands included increased duct diameter, a flattened cell morphology and reduced ductal branching (Fig. 1). This phenotype was also accompanied by reduced levels of pMLC (Fig. 2E), an indicator of decreased cell contractility and consistent with the well-established role for paxillin in organizing the F-actin cytoskeleton in mesenchymal cells (Brown and Turner, 2004; Deakin and Turner, 2008). Paxillin interacts with the FAK-Src complex at focal adhesions in response to integrin-mediated extracellular matrix signals in fibroblasts via its LD motifs to regulate pMLC-dependent contractility and coordinate cell motility (Brown and Turner, 2004; Deakin and Turner, 2008; Turner et al., 1999; Webb et al., 2004), and we also observed defects in β1 integrin and FAK signaling in the paxillin$^{fl/fl}$;cre mammary gland tissue (Fig. S2). However, work by others indicated that β1 integrin knockout in the mammary gland did not produce any ductal outgrowth defects (White et al., 2004). On the other hand, a FAK conditional knockout in mammary luminal epithelial cells resulted in reduced branching through cell proliferation defects (Nagy et al., 2007), whereas in another mammary epithelial cell (MEC) transplantation model, FAK knockout caused increased duct size and reduced organoid branching similar to our observations. However, the FAK

Development (2019) 146, dev174367. doi:10.1242/dev.174367

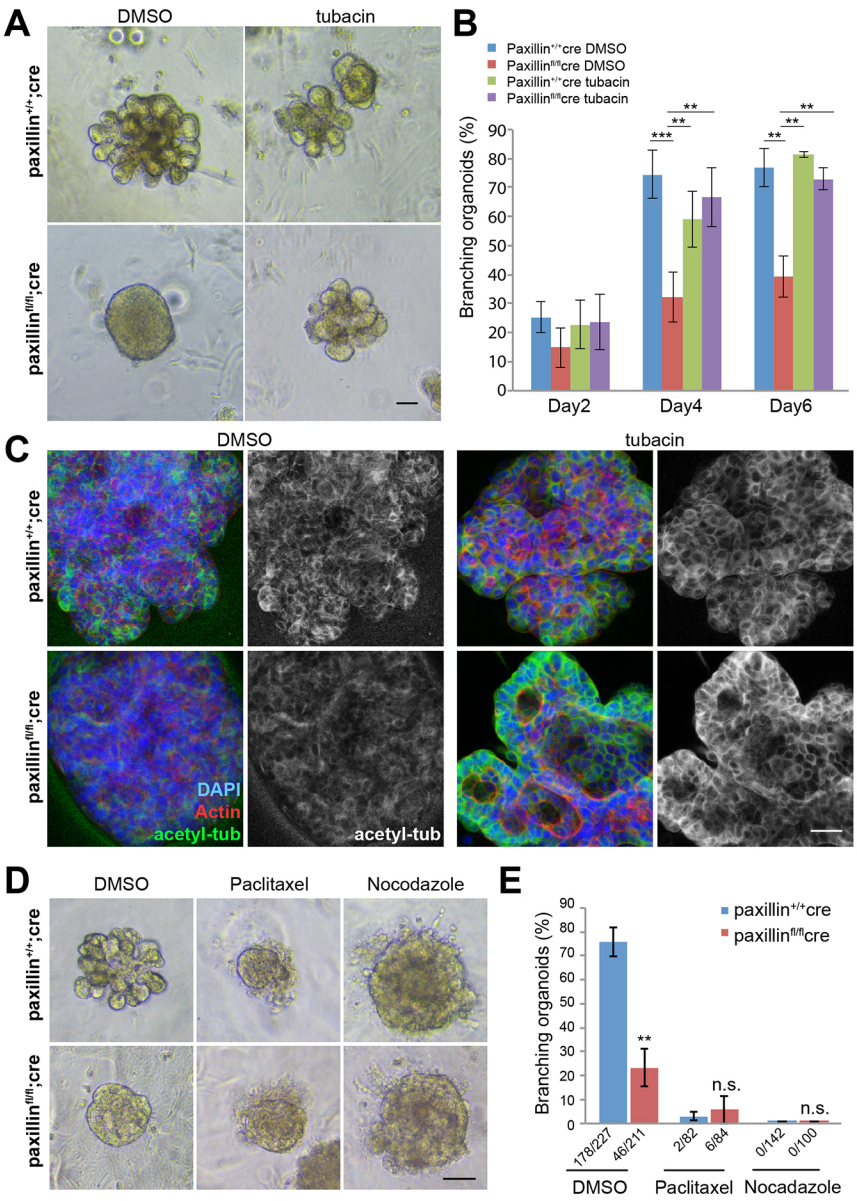

Fig. 7. Tubacin treatment rescues organoid branching in paxillin$^{fl/fl}$cre organoids. (A) Phase images of day 6 organoids treated with 2 µM tubacin for 4 days. Scale bar: 40 µm. (B) Quantification of branching at day 2, day 4 and day 6, *n*=3 (total of 18-82 organoids per treatment). One-way ANOVA with Tukey's multiple comparisons test was performed for statistical analysis. (C) Whole-mount staining of organoids showing paxillin and acetylated-tubulin expression patterns in the tubacin-treated organoids and DMSO-treated controls. Scale bar: 20 µm. (D) Phase images of 0.1 µM paclitaxel-, 200 ng/ml nocodazole- and DMSO-treated paxillin$^{+/+}$cre and paxillin$^{fl/fl}$cre organoids. Scale bar: 20 µm. (E) Quantification of branching in drug-treated organoids, *n*=3. Student's *t*-test was performed. Data are mean ±s.e.m. n.s., not significant; ***P*<0.01, ****P*<0.001.

knockout phenotype was suggested to be the result of enhanced Rho kinase (ROCK)-mediated contractility within the myoepithelium (van Miltenburg et al., 2009) and ROCK-inhibited wild-type and FAK knockout mammary organoids also resulted in a hyperbranching phenotype (Ewald et al., 2008; van Miltenburg et al., 2009). In the current study, we observed decreased levels of pMLC in luminal epithelial cells, suggesting reduced contractility in the absence of paxillin (Fig. 2E). Thus, the reason for the duct dilation/branching deficiency, caused by the loss of paxillin in mammary luminal epithelial cells, may be independent of integrin or FAK-mediated ROCK signaling. Furthermore, inhibition of myosin II by blebbistatin in the paxillin$^{fl/fl}$;cre organoids failed to rescue branching (Fig. S9A,B), suggesting that in the absence of paxillin from the luminal cells, reduced contractility in the adjacent myoepithelial cells is not sufficient to promote branching. Hence, paxillin is likely to regulate duct size/branching through F-actin cytoskeleton organization in addition to contractility in the luminal epithelial cells.

The paxillin-depleted ducts and isolated acini also exhibited increased F-actin-associated membrane blebbing, further suggesting perturbed actin dynamics or actin-membrane interactions (Figs 2C and 4H). Interestingly, at early time points the blebbing phenotype was observed in both control and paxillin-depleted acini (Fig. 4I), indicating that a highly dynamic actin cytoskeleton is required for establishing correct tissue architecture, but is subsequently deactivated via a paxillin-mediated process. A similar F-actin blebbing phenotype was observed following overexpression of a constitutively active cofilin mutant in 3D cultured Caco-2 cysts (Ivanov et al., 2008). Paxillin could potentially influence cofilin mediated F-actin assembly via TESK, which phosphorylates cofilin and can bind indirectly to paxillin through its association with actopaxin (α-parvin) (LaLonde et al., 2005).

In the paxillin$^{fl/fl}$;cre mammary gland and organoids, cell shape is perturbed (Figs 2A,B and 6D-G). Indeed, as cell proliferation was unaffected, the flattened cell shape could account for the dilated duct phenotype, combined with similar duct penetration in paxillin$^{fl/fl}$;cre mammary gland (Fig. 1A,C-F). Cell shape is also an important driver of duct branching. For example, epithelial cells with a high degree of apical constriction are associated with new branch formation on the side of a duct, while cells with a constricted

Development (2019) 146, dev174367. doi:10.1242/dev.174367

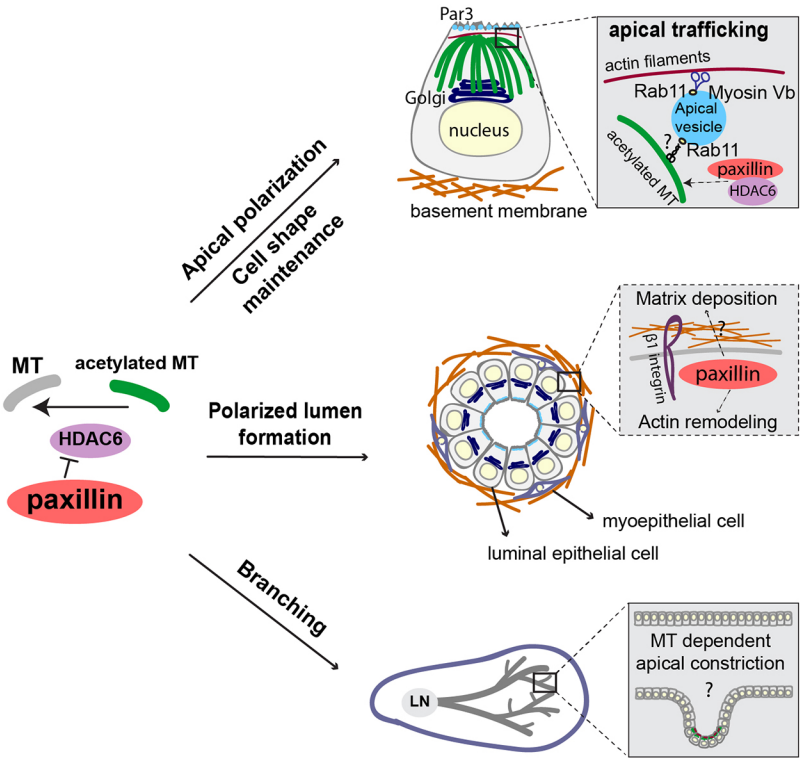

Fig. 8. Potential model for paxillin-mediated MT acetylation in the regulation of apical polarity and branching morphogenesis. During mammary gland morphogenesis, our data suggest that paxillin inhibits the α-tubulin deacetylase HDAC6 to enhance tubulin acetylation. Apically enriched acetylated MTs provide stable tracks for Rab11-dependent apical vesicles trafficking, which likely contributes to the apical accumulation of Par complex proteins. Paxillin may also assist in MyoVb stabilization of the apical membrane-associated actin network. Meanwhile, as in mesenchymal cells, paxillin-dependent MT acetylation also coordinates Golgi apical positioning and provides a more stable MT cytoskeleton to support and maintain a columnar cell shape, and aid in apical constriction. In addition, through a mechanism yet to be determined (indicated by '?' in the dashed box), paxillin-mediated regulation of inside-out integrin-based signaling contributes to matrix deposition at the basal surface, perhaps to facilitate mechanosignaling within the F-actin cytoskeleton to control lumen size. The polarized and columnar shaped epithelial cells, combined with directed trafficking, contribute to lumen formation. Additional acetylated MT-mediated epithelial cell constriction potentially facilitates branching of the ducts.

basal surface are correlated with duct bifurcation (Shih et al., 2016; Sumigray et al., 2018). Overall cell shape is dependent on the organization of both the F-actin and MT cytoskeleton networks (Dogterom and Koenderink, 2019), but their respective importance remains to be determined. Our current studies have revealed a defect in the apical enrichment of MT acetylation in the developing mammary gland in the absence of paxillin (Fig. 2F,G), while the total microtubule distribution and level is largely unaffected (Fig. S4). MT acetylation is thought to not only stabilize MTs (Takemura et al., 1992), but also increases MT resistance to mechanical breakage (Xu et al., 2017), which in turn could provide increased structural support to maintain cell shape. Although the role of MT acetylation in shaping the mammary gland has not previously been evaluated, analysis of the *Drosophila* eye disc epithelium revealed that integrins regulate actomyosin-dependent apical constriction of the epithelial cells by promoting MT minus end stability with associated elevated levels of acetylated MTs (Fernandes et al., 2014). However, the mechanism by which the basal surface-localized integrin regulates MT acetylation within the apical domain is not known. Together, our data suggest that the involvement of paxillin in both inside-out and outside-in ECM-integrin signaling, combined with its inhibition of HDAC6 activity to promote MT acetylation, could coordinate ECM signals and apical constriction to maintain proper cell shape and, in turn, coordinate the branching process (Fig. 8).

Cell-ECM signaling-dependent matrix deposition is also important for promoting branching and maintaining mammary gland organization (Fata et al., 2004; Rozen et al., 2003). Although epithelial tissues do not typically form classical focal adhesions *in vivo*, the disruption of active integrin β1 distribution and laminin deposition that was observed in the paxillin-depleted mammary glands (Fig. S2) suggests a potential defect in inside-out integrin-ECM signaling, which in turn could cause further disruption of the actin cytoskeleton organization (Figs 2C, 4H; Fig. 8). Interestingly, paxillin has been shown to perform a similar role in regulating matrix deposition during myotendinous junction formation in the developing zebrafish somites (Jacob et al., 2017).

The establishment of apical-basal polarity is a core requirement of epithelial tissue organization and function (Bryant et al., 2010). Our *in vivo* animal model and 3D culture models demonstrate that the paxillin$^{fl/fl}$;cre mammary gland is defective in numerous facets of apical-basal polarity, including dispersed Golgi apparatus and Par3 protein (Figs 3A-E and 4B,E), reduced and disorganized MT acetylation (Figs 2F-H and 4B), and mislocalized Rab11-MyoVb apical trafficking complex, which is necessary for the delivery of apical membrane proteins (Figs 3F-I and 4C,D,F,G). Importantly, paxillin depletion in mesenchymal cells also causes disruption of the positioning and integrity of the Golgi complex and front-rear polarized trafficking as a result of dysregulation of HDAC6 activity and specifically through its control of MT acetylation (Deakin and Turner, 2014; Dubois et al., 2018). We propose a similar paxillin-dependent HDAC6-MT acetylation regulation mechanism in establishing epithelial apical-basal cell polarity, as tubacin treatment rescued paxillin$^{fl/fl}$;cre acini polarity, including Golgi complex cohesion and positioning, as well as single lumen formation, while also re-establishing apical MT acetylation to wild-type levels (Fig. 5B,C; Fig. S8). Nevertheless, HDAC6 has additional substrates to α-tubulin, with cortactin and Hsp90 being the major ones (Valenzuela-Fernández et al., 2008). This raises the formal possibility that these substrates may also be associated with the regulation of apical-basal polarity by paxillin. Importantly, however, cortactin acetylation inhibits its F-actin binding activity and regulation of Arp 2/3 F-actin branching (Schnoor et al., 2017). Given that Arp2/3 activity is required for polarized lumen formation and apical protein maintenance (Bernadskaya et al., 2010; Mangan et al., 2016), we speculate that cortactin acetylation is not contributing to the rescue in paxillin$^{fl/fl}$;cre acini.

Interestingly tubacin also rescued Rab11-MyoVb distribution to the apical surface of the acini (Fig. 5D-G), which suggests that the

Development (2019) 146, dev174367. doi:10.1242/dev.174367

acetylated MT network is necessary and sufficient for Rab11-dependent apical trafficking, possibly via stabilizing or optimizing MT motor binding and/or activity (Welz et al., 2014). Alternatively, MT acetylation could be required to facilitate motor protein switching from kinesin to MyoVb at the apical membrane, or regulate F-actin-dependent apical constriction to retain MyoVb-associated vesicles at the apical surface to aid in apical domain formation (Fig. 8) (Welz et al., 2014). Additionally, in the paxillin$^{fl/fl}$;cre mammary gland, Rab11 but not MyoVb protein levels were reduced (Fig. S5). This suggests that Rab11 expression may also be regulated by paxillin or, alternatively, Rab11 may be targeted for lysosomal degradation. Rab11 is crucial for vesicle transportation from the basal to the apical membrane (Xu et al., 2013). Although Rab11 is still apically localized in the paxillin$^{fl/fl}$;cre mammary gland, the reduced level of Rab11 protein likely impacts the efficiency of apical protein translocation and thereby contributes to the failure of apical domain formation.

Although numerous studies have been performed to understand branching morphogenesis or lumen formation during mammary gland development, little is known about the relationship between these two processes. In addition to rescuing acini polarity and single lumen formation, tubacin treatment also rescued the branching defect in the paxillin$^{fl/fl}$;cre organoids (Fig. 7A,B), suggesting that paxillin-regulated MT acetylation is also key to controlling branching morphogenesis. These data further suggest that MT acetylation-dependent polarized lumen formation is a prerequisite for branching and that MT acetylation-dependent mechanical support, which is necessary for cell shape maintenance, is also key to promoting optimal duct organization and branching (Fig. 8).

In summary, the analysis described herein identifies paxillin as a central regulator of multiple aspects of mammary gland morphogenesis. Importantly, despite the multiple pathways through which paxillin could potentially regulate apical-basal polarity and branching morphogenesis, the common rescue by tubacin treatment of the major developmental defects observed after paxillin depletion, greatly focuses attention on the role of microtubule acetylation and emphasizes the importance of the paxillin-HDAC6-MT acetylation signaling axis (Fig. 8). Furthermore, this new conditional knockout animal model provides a foundation for further assessment of the mechanism(s) by which paxillin regulates mammary gland function, e.g. in the context of tissue remodeling during pregnancy to support milk production or evaluation of its role in breast cancer progression.

MATERIALS AND METHODS

Animals

All mouse experiments were performed in compliance with protocols approved by SUNY Upstate Medical University IACUC. The paxillin$^{fl/fl}$ mice were generated as previously described (Rashid et al., 2017). Paxillin$^{fl/+}$ mice were crossed with transgenic MMTV-LTRcre mice (strain D, JAX stock #003553) (Wagner et al., 2001) to produce paxillin$^{+/+}$;cre and paxillin$^{fl/fl}$;cre mice. Paxillin$^{fl/+}$ mice were maintained on a mixed genetic background (C57BL/6J and FVB/N). Mammary glands isolated from 6-week-old mice were used for immunohistochemistry (IHC) analysis. Female mice between 10 and 14 weeks of age were used for tissue isolation, and for organoid branching and acini formation experiments.

Histology

Whole-mount analysis was performed by staining the fourth inguinal mammary glands with carmine alum, as described previously (Goreczny et al., 2017). For quantification of branch number, both bifurcation and lateral branching was counted. The counting was initiated at the lymph node and extended to the terminal end buds. For stalk length quantification, we used the ImageJ segmented line tool plug-in. Mammary glands were fixed in 4% paraformaldehyde, embedded in OCT and sectioned (6 µm). Tissue sections were subjected to standard H&E staining. A Zeiss Axioskop2 plus microscope fitted with a QImaging EXi Blue charge-coupled device camera and Plan-Apochromat 10× or 20× objectives was used to image tissue sections. The images were analyzed as described below using ImageJ.

3D organotypic assay

Three-dimensional (3D) organoids were prepared as previously described (Nguyen-Ngoc et al., 2015). Briefly, mammary glands were minced and shaken for 45-60 min at 37°C in digestion media [2 mg/ml collagenase (C2139; Sigma Aldrich), 2 mg/ml trypsin (85450C; Sigma), 5 µg/ml insulin (I9278; Sigma), 5% v/v fetal bovine serum and 1% v/v penicillin/streptomycin in DMEM/F12]. The dissociated tissue solution was centrifuged at 400 ***g*** for 10 min, and the pellet was resuspended in 4 ml DMEM/F12 plus 40 µl DNase (2 U/µl; D4263; Sigma). The DNase solution was shaken by hand for 2-5 min and centrifuged at 400 ***g*** for 10 min. The organoids were pelleted by brief centrifugation at 400 ***g***.

Organoid branching morphogenesis was performed in 24-well plates. Organoids were suspended in Matrigel (354234; Corning) at a density of 1000 organoids/ml. Aliquots of the organoid suspension (100 µl) were added to each well of a 24-well plate and allowed to solidify for 20 min at 37°C. FGF2/branching media [DMEM/F12, 1% v/v insulin-transferrin-selenium-X (ITS) (51500; Gibco), 1% v/v penicillin/streptomycin (30-002-CI; Corning) and 2.5 nM FGF2 (F0291; Sigma)] was added to the Matrigel-embedded organoids. Organoids were tracked by taking phase-contrast images every day for at least 7 days. For quantitation, organoids with more than four branches were scored as being branched.

Primary cell culture and 3D acini formation

Primary mammary epithelial cells were isolated and cultured as previously described with minor modifications (Akhtar and Streuli, 2013). Briefly, cells were plated onto collagen I-coated 10 cm plastic dishes for monolayer cultures for one passage, and then replated onto Matrigel-coated coverslips in acini culture media (DMEM/F12, 5 µg/ml insulin, 1 µg/ml hydrocortisone, 3 ng/ml EGF, 10% FBS, 1% v/v penicillin/streptomycin, 1% Matrigel) for 6 days to form acini. For acini polarity quantification, an acinus with more than 90% apical Golgi staining was counted as polarized. For lumen number quantification, ZO-1 staining surrounding a void was counted as a lumen.

Drug treatment

Organoids and/or acini were treated with the HDAC6 inhibitor tubacin (2 µM) (SML0065; MilliporeSigma), the microtubule depolymerizing drug nocodazole (200 ng/ml, 20 ng/ml and 2 ng/ml) (487928; MilliporeSigma), the microtubule disassembly inhibitor paclitaxel (0.1 µM, 10 nM and 1 nM) (T7191; MilliporeSigma) and the myosin II inhibitor blebbistatin (10-50 µM) (203390; MilliporeSigma). For the organoids, drugs were added at day 2 and treated for 4 days. For acini, drugs were added at day 4 and treated for 2 days. Organoids and acini were fixed 6 days after culturing for further analyses.

FM4-64 lipophilic dye transport assay

FM4-64 dye (T13320; ThermoFisher, Waltham, MA, USA) was dissolved in DMSO and stored at −20°C as a 10 mM stock solution. For live-cell imaging, 6-day acini were treated with 2.5 µg/ml FM4-64 dye for 10 min on ice. Live-cell imaging was performed every 5 min for 2 h at 37°C in 5% CO_2 using a Leica SP8 scanning confocal microscope with a high-contrast Plan-Apochromat CS2 20×/0.75 IMM objective.

Antibodies and reagents

Antibodies used were anti-paxillin (1:100 for immunostaining, 1:1000 for western blotting, H114; Santa Cruz Biotechnology), anti-Par-3 (1:100, 07-330; EMD Millipore), anti-giantin (1:400, PRB-114C; Covance), anti-HDAC6 (1:1000, H2287; Sigma), anti-Laminin (1:100, L9393, Sigma), anti-α-tubulin (1:100, T9026, Sigma), anti-α-SMA (1:200, A5228; Sigma), anti-GM130 (1:100, G65120; BD Biosciences), anti-E-cadherin (1:100, 610182; BD Biosciences), anti-CD29 clone 9EG7 (1:10, 553715; BD Biosciences), anti-FAK (1:1000, 610087; BD Biosciences), anti-Rab11

(1:100 for immunostaining, 1:1000 for western blotting, 5589; Cell Signaling), anti-acetyl-α-tubulin (1:100 for immunostaining, 1:1000 for western blotting, 5335; Cell Signaling), anti-pMLC (1:1000, 3671; Cell Signaling), anti-cleaved caspase 3 (1:100, 9661; Cell Signaling), anti-Slug (1:100, 9585; Cell Signaling), anti-myosin Vb (1:100 for immunostaining, 1:1000 for western blotting, NBP1-87746; Novus Biologicals), anti-EpCAM (1:200) (Developmental Studies Hybridoma Bank, University of Iowa), anti-Ki67 (1:100, 15580; Abcam), anti-FAK/PYK2 pTyr397 (1:1000, 700255; Invitrogen) and anti-ZO-1 (1:100, 40-2200; Invitrogen) Rhodamine-phalloidin (R415; ThermoFisher) was used to visualize F-actin; DAPI (D9542; Sigma) was used to visualize nuclei. Secondary antibodies used were DyLight 488-conjugated goat anti-mouse (1:250, 35502; Thermo Fisher), DyLight 550-conjugated goat anti-mouse (1:250, 84540; Thermo Fisher), DyLight 488-conjugated goat anti-rabbit (1:250, 35552; Thermo Fisher), DyLight 550-conjugated goat anti-rabbit (1:250, 84541; Thermo Fisher) and Alexa Fluor 488 AffiniPure goat anti-rat (1:250, 112-545-003; Jackson ImmunoResearch).

Immunostaining

Mammary gland cryosections were washed in phosphate-buffered saline (PBS) and blocked in 10% normal goat serum for 2 h. Antibodies were diluted in 10% normal goat serum in PBS. Sections were incubated at 4°C overnight, washed in PBS+0.1% TX-100 (PBST), followed by 2 h incubation in secondary antibody. F-actin was detected by incubating sections with rhodamine-phalloidin and nuclei were stained with DAPI.

Organoids cryosections or 3D-cultured whole acini were washed in PBS and blocked in 3% bovine serum albumin (BSA) for 1 h. Antibodies were diluted in 3% BSA in PBS. Slides were incubated at 37°C for 2 h, washed in PBS+0.1% TX-100 (PBST), followed by 1 h incubation in secondary antibody. F-actin was stained with rhodamine-phalloidin, and nuclei were stained with DAPI.

Organoid whole-mount staining was performed as previously described (Ewald et al., 2008). Briefly, organoids were fixed with 4% paraformaldehyde (PFA) at 4°C overnight, washed with PBS and blocked with 3% BSA for 24 h. Antibodies were diluted in 3% BSA. Organoids were incubated in primary antibody at 4°C for 2 days, washed with PBST for a day, followed by a 1-day incubation in secondary antibody. F-actin or DAPI were incubated for 1 h. Images were acquired using either a Leica SP8 scanning confocal or Zeiss Axioskop2 plus microscope as above.

Imaris analysis

Image analysis of 3D cell shape was performed using Imaris x64 version 9.0.1 (Bitplane). The phalloidin stained images of the organoids were autosegmented using the default cell membrane detection algorithm. The $\text{ellipticity}_{\text{oblate}}$ of at least 200 cells within a single plane of the organoid was quantified using the equation

$$e_{\text{oblate}} = \{2b^2/(b^2 + c^2)\} \times \{1 - (2a^2/(b^2 + c^2))\}.$$

The line segments from the origin to points (a,0,0), (0,b,0) and (0,0,c), which lie on the surface, are the principal semi-axes of the ellipsoid, and a, b, c are half the length of the principal axes. a=b<c defines a prolate spheroid; a<b=c defines an oblate spheroid.

ImageJ analysis

Line profile analysis was performed using ImageJ and the ratio of the maximum fluorescence intensity at the apical membrane to the maximum fluorescence intensity at the basal membrane of a cell was determined. Individual cells in the ducts were thresholded and evaluated using the 'analyze particles' ImageJ plug-in to measure Rab11 mean fluorescence intensity (MFI). For laminin levels, laminin MFI was normalized to the α-smooth muscle actin MFI. For acetylated MT levels, acetyl-tubulin MFI was normalized to GM130.

Immunoblotting

Six-week-old mammary glands or one passage primary mammary epithelial cells (MECs) were lysed in sample buffer [20 mM Tris-HCl (pH 8), 10% glycerol, 2% SDS and 0.1% bromophenol blue]. Tissue/cell lysates were electrophoresed through 10% SDS polyacrylamide gels and transferred to nitrocellulose (Life Science). The membranes were blocked and probed with primary and secondary antibodies, as indicated, and then visualized and quantified by chemiluminescence (SuperSignal West; Thermo Fisher Scientific) using a Chemidoc MP imaging system (Bio-Rad).

Statistical analysis

All data were analyzed using a two-sided Student's *t*-test or one-way ANOVA with post-hoc test, as indicated. All data were generated from at least three independent mice for each condition. Statistical significance is indicated by $*P<0.05$, $**P<0.01$, $***P<0.001$. Data are mean±s.e.m.

Acknowledgements

We thank the members of the Turner lab for insightful discussions. We thank Ian Forsythe, Kyle Alpha and Theresa Stowell for assistance with mouse husbandry and genotyping.

Competing interests

The authors declare no competing or financial interests.

Author contributions

Conceptualization: W.X., C.E.T.; Formal analysis: W.X., A.C.G., G.J.G., C.E.T.; Investigation: W.X., C.E.T.; Writing - original draft: W.X., C.E.T.; Writing - review & editing: W.X., A.C.G., G.J.G., E.C.O., C.E.T.; Supervision: C.E.T.; Funding acquisition: C.E.T.

Funding

This work was supported by the National Institutes of Health (RO1 GM047607 to C.E.T.). Deposited in PMC for release after 12 months.

Supplementary information

Supplementary information available online at
http://dev.biologists.org/lookup/doi/10.1242/dev.174367.supplemental

References

Ahmed, S. M. and Macara, I. G. (2017). The Par3 polarity protein is an exocyst receptor essential for mammary cell survival. *Nat. Commun.* **8**, 14867. doi:10.1038/ncomms14867

Akhtar, N. and Streuli, C. H. (2006). Rac1 links integrin-mediated adhesion to the control of lactational differentiation in mammary epithelia. *J. Cell Biol.* **173**, 781-793. doi:10.1083/jcb.200601059

Akhtar, N. and Streuli, C. H. (2013). An integrin-ILK-microtubule network orients cell polarity and lumen formation in glandular epithelium. *Nat. Cell Biol.* **15**, 17-27. doi:10.1038/ncb2646

Akhtar, N., Marlow, R., Lambert, E., Schatzmann, F., Lowe, E. T., Cheung, J., Katz, E., Li, W., Wu, C., Dedhar, S. et al. (2009). Molecular dissection of integrin signalling proteins in the control of mammary epithelial development and differentiation. *Development* **136**, 1019-1027. doi:10.1242/dev.028423

Andrew, D. J. and Ewald, A. J. (2010). Morphogenesis of epithelial tubes: insights into tube formation, elongation, and elaboration. *Dev. Biol.* **341**, 34-55. doi:10.1016/j.ydbio.2009.09.024

Bernadskaya, Y. Y., Patel, F. B., Hsu, H.-T. and Soto, M. C. (2010). Arp2/3 promotes junction formation and maintenance in the Caenorhabditis elegans intestine by regulating membrane association of apical proteins. *Mol. Biol. Cell* **22**, 2886-2899. doi: 10.1091/mbc.E10-10-0862

Bilder, D. and Perrimon, N. (2000). Localization of apical epithelial determinants by the basolateral PDZ protein Scribble. *Nature* **403**, 676-680. doi:10.1038/35001108

Booth, A. J. R., Blanchard, G. B., Adams, R. J. and Röper, K. (2014). A dynamic microtubule cytoskeleton directs medial actomyosin function during tube formation. *Dev. Cell* **29**, 562-576. doi:10.1016/j.devcel.2014.03.023

Brown, M. C. and Turner, C. E. (2004). Paxillin: adapting to change. *Physiol. Rev.* **84**, 1315-1339. doi:10.1152/physrev.00002.2004

Bryant, D. M., Datta, A., Rodríguez-Fraticelli, A. E., Peränen, J., Martín-Belmonte, F. and Mostov, K. E. (2010). A molecular network for de novo generation of the apical surface and lumen. *Nat. Cell Biol.* **12**, 1035-1045. doi:10.1038/ncb2106

Bryant, D. M., Roignot, J., Datta, A., Overeem, A. W., Kim, M., Yu, W., Peng, X., Eastburn, D. J., Ewald, A. J., Werb, Z. et al. (2014). A molecular switch for the orientation of epithelial cell polarization. *Dev. Cell* **31**, 171-187. doi:10.1016/j.devcel.2014.08.027

Datta, A., Bryant, D. M. and Mostov, K. E. (2011). Molecular regulation of lumen morphogenesis. *Curr. Biol.* **21**, R126-R136. doi:10.1016/j.cub.2010.12.003

Deakin, N. O. and Turner, C. E. (2008). Paxillin comes of age. *J. Cell Sci.* **121**, 2435-2444. doi:10.1242/jcs.018044

Deakin, N. O. and Turner, C. E. (2014). Paxillin inhibits HDAC6 to regulate microtubule acetylation, Golgi structure, and polarized migration. *J. Cell Biol.* **206**, 395-413. doi:10.1083/jcb.201403039

Dogterom, M. and Koenderink, G. H. (2019). Actin-microtubule crosstalk in cell biology. *Nat. Rev. Mol. Cell Biol.* **20**, 38-54. doi:10.1038/s41580-018-0067-1

Dubois, F., Alpha, K. and Turner, C. E. (2018). Paxillin regulates cell polarization and anterograde vesicle trafficking during cell migration. *MBoC* **28**, 3815-3831. doi:10.1091/mbc.e17-08-0488

Elias, S., McGuire, J. R., Yu, H. and Humbert, S. (2015). Huntingtin is required for epithelial polarity through RAB11A-mediated apical trafficking of PAR3-aPKC. *PLoS Biol.* **13**, e1002142. doi:10.1371/journal.pbio.1002142

Ewald, A. J., Brenot, A., Duong, M., Chan, B. S. and Werb, Z. (2008). Collective epithelial migration and cell rearrangements drive mammary branching morphogenesis. *Dev. Cell* **14**, 570-581. doi:10.1016/j.devcel.2008.03.003

Fata, J. E., Werb, Z. and Bissell, M. J. (2004). Regulation of mammary gland branching morphogenesis by the extracellular matrix and its remodeling enzymes. *Breast Cancer Res.* **6**, 1-11. doi: 10.1186/bcr634

Fernandes, V. M., McCormack, K., Lewellyn, L. and Verheyen, E. M. (2014). Integrins regulate apical constriction via microtubule stabilization in the Drosophila eye disc epithelium. *Cell Rep.* **9**, 2043-2055. doi:10.1016/j.celrep.2014.11.041

Gjorevski, N. and Nelson, C. M. (2010). Endogenous patterns of mechanical stress are required for branching morphogenesis. *Integr. Biol.* **2**, 424-434. doi:10.1039/c0ib00040j

Goreczny, G. J., Ouderkirk-Pecone, J. L., Olson, E. C., Krendel, M. and Turner, C. E. (2017). Hic-5 remodeling of the stromal matrix promotes breast tumor progression. *Oncogene* **36**, 2693-2703. doi:10.1038/onc.2016.422

Guo, W., Keckesova, Z., Donaher, J. L., Shibue, T., Tischler, V., Reinhardt, F., Itzkovitz, S., Noske, A., Zürrer-Härdi, U., Bell, G. et al. (2012). Slug and Sox9 cooperatively determine the mammary stem cell state. *Cell* **148**, 1015-1028. doi:10.1016/j.cell.2012.02.008

Hagel, M., George, E. L., Kim, A., Tamimi, R., Opitz, S. L., Turner, C. E., Imamoto, A. and Thomas, S. M. (2002). The adaptor protein Paxillin is essential for normal development in the mouse and is a critical transducer of fibronectin signaling. *Mol. Cell. Biol.* **22**, 901-915. doi:10.1128/MCB.22.3.901-915.2002

Haggarty, S. J., Koeller, K. M., Wong, J. C., Grozinger, C. M. and Schreiber, S. L. (2003). Domain-selective small-molecule inhibitor of histone deacetylase 6 (HDAC6)-mediated tubulin deacetylation. *Proc. Natl. Acad. Sci. USA* **100**, 4389-4394. doi:10.1073/pnas.0430973100

Ivanov, A. I., Hopkins, A. M., Brown, G. T., Gerner-Smidt, K., Babbin, B. A., Parkos, C. A. and Nusrat, A. (2008). Myosin II regulates the shape of three-dimensional intestinal epithelial cysts. *J. Cell Sci.* **121**, 1803-1814. doi:10.1242/jcs.015842

Jacob, A. E., Amack, J. D. and Turner, C. E. (2017). Paxillin genes and actomyosin contractility regulate myotome morphogenesis in zebrafish. *Dev. Biol.* **425**, 70-84. doi:10.1016/j.ydbio.2017.03.012

Kadoya, Y. and Yamashina, S. (2010). Cellular dynamics of epithelial clefting during branching morphogenesis of the mouse submandibular gland. *Dev. Dyn.* **239**, 1739-1747. doi:10.1002/dvdy.22312

Kapitein, L. C., van Bergeijk, P., Lipka, J., Keijzer, N., Wulf, P. S., Katrukha, E. A., Akhmanova, A. and Hoogenraad, C. C. (2013). Myosin-V opposes microtubule-based cargo transport and drives directional motility on cortical actin. *Curr. Biol.* **23**, 828-834. doi:10.1016/j.cub.2013.03.068

Kim, E. J. Y., Korotkevich, E. and Hiiragi, T. (2018). Coordination of cell polarity, mechanics and fate in tissue self-organization. *Trends Cell Biol.* **28**, 541-550. doi:10.1016/j.tcb.2018.02.008

LaLonde, D. P., Brown, M. C., Bouverat, B. P. and Turner, C. E. (2005). Actopaxin interacts with TESK1 to regulate cell spreading on fibronectin. *J. Biol. Chem.* **280**, 21680-21688. doi:10.1074/jbc.M500752200

Lloyd-Lewis, B., Harris, O. B., Watson, C. J. and Davis, F. M. (2017). Mammary stem cells: premise, properties, and perspectives. *Trends Cell Biol.* **27**, 556-567. doi:10.1016/j.tcb.2017.04.001

Lu, P., Ewald, A. J., Martin, G. R. and Werb, Z. (2008). Genetic mosaic analysis reveals FGF receptor 2 function in terminal end buds during mammary gland branching morphogenesis. *Dev. Biol.* **321**, 77-87. doi:10.1016/j.ydbio.2008.06.005

Mangan, A. J., Sietsema, D. V., Li, D., Moore, J. K., Citi, S. and Prekeris, R. (2016). Cingulin and actin mediate midbody-dependent apical lumen formation during polarization of epithelial cells. *Nat. Commun.* **7**, 12426. doi:10.1038/ncomms12426

McCaffrey, L. M. and Macara, I. G. (2009). The Par3/aPKC interaction is essential for end bud remodeling and progenitor differentiation during mammary gland morphogenesis. *Genes Dev.* **23**, 1450-1460. doi:10.1101/gad.1795909

Muschler, J. and Streuli, C. H. (2010). Cell-matrix interactions in mammary gland development and breast cancer. *Cold Spring Harb. Perspect. Biol.* **2**, a003202. doi:10.1101/cshperspect.a003202

Nagy, T., Wei, H., Shen, T.-L., Peng, X., Liang, C.-C., Gan, B. and Guan, J.-L. (2007). Mammary epithelial-specific deletion of the focal adhesion kinase gene leads to severe lobulo-alveolar hypoplasia and secretory immaturity of the murine mammary gland. *J. Biol. Chem.* **282**, 31766-31776. doi:10.1074/jbc.M705403200

Neumann, N. M., Perrone, M. C., Veldhuis, J. H., Huebner, R. J., Zhan, H., Devreotes, P. N., Brodland, G. W. and Ewald, A. J. (2018). Coordination of receptor tyrosine kinase signaling and interfacial tension dynamics drives radial intercalation and tube elongation. *Dev. Cell* **45**, 67-82.e66. doi:10.1016/j.devcel.2018.03.011

Nguyen-Ngoc, K.-V., Shamir, E. R., Huebner, R. J., Beck, J. N., Cheung, K. J. and Ewald, A. J. (2015). 3D culture assays of murine mammary branching morphogenesis and epithelial invasion. *Methods Mol. Biol.* **1189**, 135-162. doi:10.1007/978-1-4939-1164-6_10

Nikolopoulos, S. N. and Turner, C. E. (2001). Integrin-linked kinase (ILK) binding to paxillin LD1 motif regulates ILK localization to focal adhesions. *J. Biol. Chem.* **276**, 23499-23505. doi:10.1074/jbc.M102163200

Rashid, M., Belmont, J., Carpenter, D., Turner, C. E. and Olson, E. C. (2017). Neural-specific deletion of the focal adhesion adaptor protein paxillin slows migration speed and delays cortical layer formation. *Development* **144**, 4002-4014. doi:10.1242/dev.147934

Rodriguez-Boulan, E. and Macara, I. G. (2014). Organization and execution of the epithelial polarity programme. *Nat. Rev. Mol. Cell Biol.* **15**, 225-242. doi:10.1038/nrm3775

Rodriguez-Fraticelli, A. E., Galvez-Santisteban, M. and Martin-Belmonte, F. (2011). Divide and polarize: recent advances in the molecular mechanism regulating epithelial tubulogenesis. *Curr. Opin. Cell Biol.* **23**, 638-646. doi:10.1016/j.ceb.2011.07.002

Roignot, J., Peng, X. and Mostov, K. (2013). Polarity in mammalian epithelial morphogenesis. *Cold Spring Harb. Perspect. Biol.* **5**, 1-15. doi:10.1101/cshperspect.a013789

Roland, J. T., Bryant, D. M., Datta, A., Itzen, A., Mostov, K. E. and Goldenring, J. R. (2011). Rab GTPase–Myo5B complexes control membrane recycling and epithelial polarization. *Proc. Natl. Acad. Sci. USA* **108**, 2789-2794. doi:10.1073/pnas.1010754108

Rozen, S., Skaletsky, H., Marszalek, J. D., Minx, P. J., Cordum, H. S., Waterston, R. H., Wilson, R. K. and Page, D. C. (2003). Abundant gene conversion between arms of palindromes in human and ape Y chromosomes. *Nature* **423**, 873-876. doi:10.1038/nature01723

Schedin, P. and Keely, P. J. (2011). Mammary gland ECM remodeling, stiffness, and mechanosignaling in normal development and tumor progression. *Cold Spring Harb. Perspect. Biol.* **3**, a003228. doi:10.1101/cshperspect.a003228

Schnoor, M., Stradal, T. E. and Rottner, K. (2017). Cortactin: cell functions of a multifaceted actin-binding protein. *Trends Cell Biol.* **28**. doi:10.1016/j.tcb.2017.10.009

Shih, H. P., Panlasigui, D., Cirulli, V. and Sander, M. (2016). ECM signaling regulates collective cellular dynamics to control pancreas branching morphogenesis. *Cell Rep.* **14**, 169-179. doi:10.1016/j.celrep.2015.12.027

Simian, M., Hirai, Y., Navre, M., Werb, Z., Lochter, A. and Bissell, M. J. (2001). The interplay of matrix metalloproteinases, morphogens and growth factors is necessary for branching of mammary epithelial cells. *Development* **128**, 3117-3131.

Song, Y. and Brady, S. T. (2015). Post-translational modifications of tubulin: pathways to functional diversity of microtubules. *Trends Cell Biol.* **25**, 125-136. doi:10.1016/j.tcb.2014.10.004

Spurlin, J. W., III and Nelson, C. M. (2017). Building branched tissue structures: from single cell guidance to coordinated construction. *Philos. Trans. R. Soc. Lond. B Biol. Sci.* **372**, 1-15. doi:10.1098/rstb.2015.0527

Sumigray, K. D., Terwilliger, M. and Lechler, T. (2018). Morphogenesis and Compartmentalization of the Intestinal Crypt. *Dev. Cell* **45**, 183-197.e185. doi:10.1016/j.devcel.2018.03.024

Takemura, R., Okabe, S., Umeyama, T., Kanai, Y., Cowan, N. J. and Hirokawa, N. (1992). Increased microtubule stability and alpha tubulin acetylation in cells transfected with microtubule-associated proteins MAP1B, MAP2 or tau. *J. Cell Sci.* **103**, 953-964.

Tepass, U., Theres, C. and Knust, E. (1990). crumbs encodes an EGFlike protein expressed on apical membranes of Drosophila epithelial cells and required for organization of epithelia. *Cell* **61**, 787-799. doi:10.1016/0092-8674(90)90189-L

Turner, C. E. (2000). Paxillin and focal adhesion signalling. *Nat. Cell Biol.* **2**, E231-E236. doi:10.1038/35046659

Turner, C. E. and Miller, J. T. (1994). Primary sequence of paxillin contains putative SH2 and SH3 domain binding motifs and multiple LIM domains: identification of a vinculin and pp125Fak- binding region. *J. Cell Sci.* **107**, 1583-1591.

Turner, C. E., Glenney, J. R. and Burridge, K. (1990). Paxillin: a new vinculin-binding protein present in focal adhesions. *J. Cell Biol.* **111**, 1059-1068. doi:10.1083/jcb.111.3.1059

Turner, C. E., Brown, M. C., Perrotta, J. A., Riedy, M. C., Nikolopoulos, S. N., McDonald, A. R., Bagrodia, S., Thomas, S. and Leventhal, P. S. (1999). Paxillin LD4 motif binds PAK and PIX through a novel 95-kD ankyrin repeat, ARF–GAP protein: a role in cytoskeletal remodeling. *J. Cell Biol.* **145**, 851-863. doi:10.1083/jcb.145.4.851

Valenzuela-Fernández, A., Cabrero, J. R., Serrador, J. M. and Sánchez-Madrid, F. (2008). HDAC6: a key regulator of cytoskeleton, cell migration and cell-cell interactions. *Trends Cell Biol.* **18**, 291-297. doi:10.1016/j.tcb.2008.04.003

van Miltenburg, M. H. A. M., Lalai, R., de Bont, H., van Waaij, E., Beggs, H., Danen, E. H. J. and van de Water, B. (2009). Complete focal adhesion kinase deficiency in the mammary gland causes ductal dilation and aberrant branching morphogenesis through defects in Rho kinase-dependent cell contractility. *FASEB J.* **23**, 3482-3493. doi:10.1096/fj.08-123398

Wagner, K.-U., Ward, T., Davis, B., Wiseman, R. and Hennighausen, L. (2001). Spatial and temporal expression of the Cre gene under the control of the MMTV-LTR in different lines of transgenic mice. *Transgenic Res.* **10**, 545-553. doi:10.1023/A:1013063514007

Webb, D. J., Donais, K., Whitmore, L. A., Thomas, S. M., Turner, C. E., Parsons, J. T. and Horwitz, A. F. (2004). FAK-Src signalling through paxillin, ERK and MLCK regulates adhesion disassembly. *Nat. Cell Biol.* **6**, 154-161. doi:10.1038/ncb1094

Welz, T., Wellbourne-Wood, J. and Kerkhoff, E. (2014). Orchestration of cell surface proteins by Rab11. *Trends Cell Biol.* **24**, 407-415. doi:10.1016/j.tcb.2014.02.004

White, D. E., Kurpios, N. A., Zuo, D., Hassell, J. A., Blaess, S., Mueller, U. and Muller, W. J. (2004). Targeted disruption of beta1-integrin in a transgenic mouse model of human breast cancer reveals an essential role in mammary tumor induction. *Cancer Cell* **6**, 159-170. doi:10.1016/j.ccr.2004.06.025

Xu, S., Ma, L., Evans, E., Okamoto, C. T. and Hamm-Alvarez, S. F. (2013). Polymeric immunoglobulin receptor traffics through two distinct apically targeted pathways in primary lacrimal gland acinar cells. *J. Cell Sci.* **126**, 2704-2717. doi:10.1242/jcs.122242

Xu, Z., Schaedel, L., Portran, D., Aguilar, A., Gaillard, J., Marinkovich, M. P., Thery, M. and Nachury, M. V. (2017). Microtubules acquire resistance from mechanical breakage through intralumenal acetylation. *Sci. Rep.* **356**, 328-332. doi:10.1126/science.aai8764